NAA-SR-6301
TRW REPORT No. ER-4442

THE SNAP II POWER CONVERSION SYSTEM
TOPICAL REPORT No. 8
MERCURY CONDENSING RESEARCH STUDIES

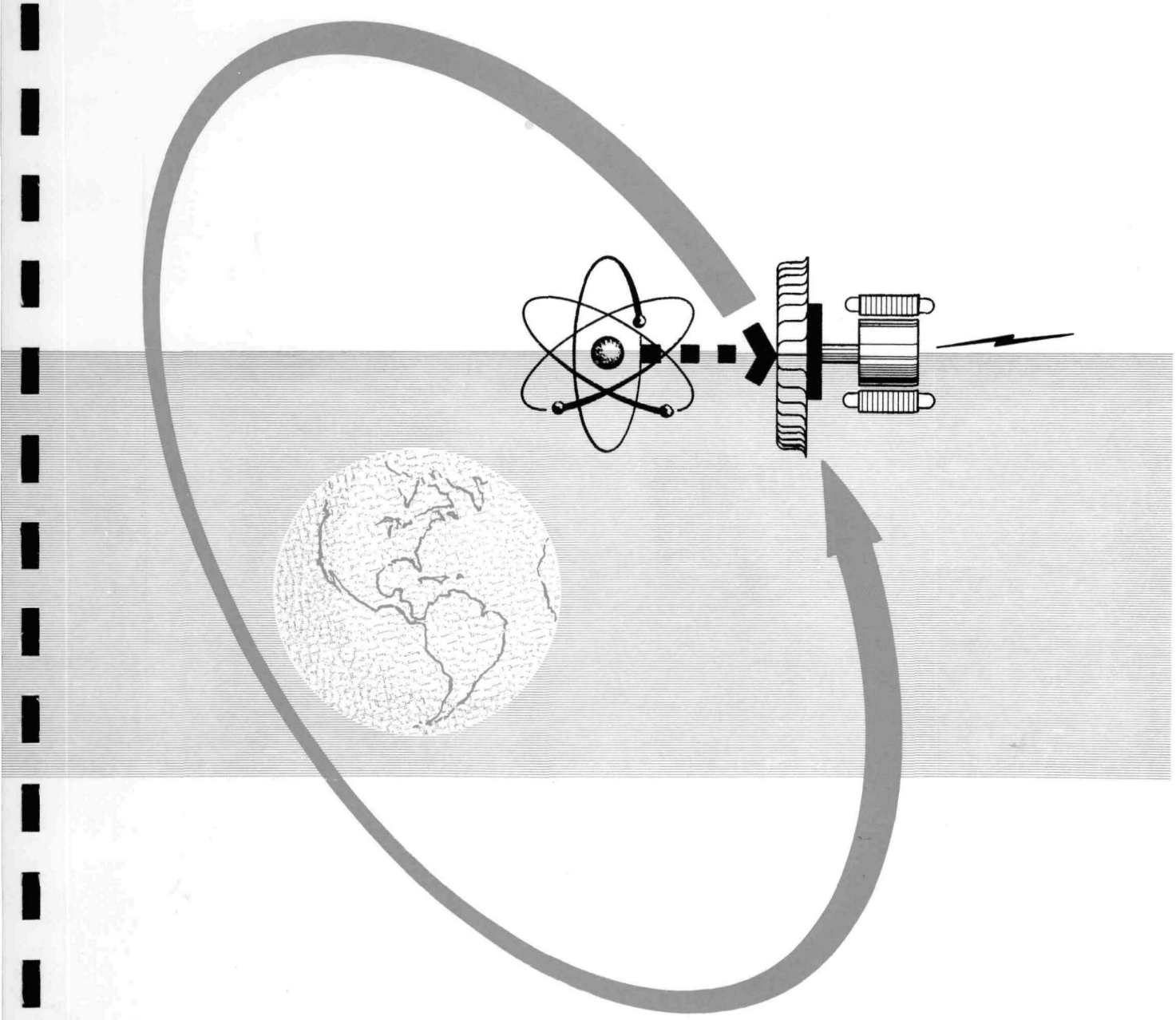

AEC RESEARCH AND DEVELOPMENT REPORT

PREPARED UNDER SUBCONTRACT
N 843 FS-101221 FOR ATOMICS
INTERNATIONAL, A DIVISION OF
NORTH AMERICAN AVIATION, INC.

TAPCO a division of
Thompson Ramo Wooldridge Inc.
CLEVELAND, OHIO

DISCLAIMER

PROJECT

512-158252-88

NAA-SR-6301
SNAP II POWER CONVERSION SYSTEM
TOPICAL REPORT NO. 8
MERCURY CONDENSING RESEARCH STUDIES
TRW REPORT NO. ER-4442

PREPARED BY:	CHECKED BY:	APPROVED BY:
R. J. Niraly Design Engineer	G. Y. Ono Senior Project Engineer	W. R. Chapman Manager, Engineering
A. Koestel Senior Engineering Specialist	D. L. Southam Project Manager	J. E. Taylor, Manager New Devices Laboratories
	R. J. Reinmann Project Engineer	

Prepared under Subcontract N843FS-101221 for Atomics International,
A Division of North American Aviation, Inc.

DATE

May 31, 1961

DEPARTMENT

0868

Thompson Ramo Wooldridge Inc.

CLEVELAND, OHIO, U. S. A.

LEGAL NOTICE

This report was prepared as an account of Government sponsored work. Neither the United States, nor the Commission, nor any person acting on behalf of the Commission:

A. Makes any warranty or representation, express or implied, with respect to the accuracy, completeness, or usefulness of the information, apparatus, method, or process disclosed in this report, or that the use of any information, apparatus, method or process disclosed in this report may not infringe privately owned rights; or

B. Assumed any liabilities with respect to the use of or for damages resulting from the use of information, apparatus, method, or process disclosed in this report.

As used in the above, "person acting on behalf of the Commission" includes any employee or contractor of the Commission to the extent that such employee or contractor prepares, handles or distributes, or provides access to, any information pursuant to his employment or contract with the Commission.

ABSTRACT

SNAP II is the designation for a 3 KW nuclear auxiliary power unit to be used in a satellite vehicle. The SNAP II system consists of a reactor heat source, a mercury Rankine engine, and an alternator. The condenser, a component of the mercury Rankine engine, returns the mercury vapor from the turbine exhaust to the liquid state, subcools the liquid, and supplies this liquid to the condensate pump. The results of the condenser research effort are presented in this report. This work was performed under a subcontract to Atomics International as part of the Atomic Energy Commission Contract AT (11-1)-GEN-8.

SUMMARY

Space radiator-condensers not only constitute a major portion of the weight of a power plant system, but also present a major portion of the zero-gravity, two-phase, fluid mechanic problem areas. A considerable research effort was expended during the 1959-1960 fiscal year in condenser fluid mechanics. This report summarizes the findings from experimentation.

Correlated two-phase pressure drop data are presented in the form of Φ (ratio of pressure drop when both liquid and gas or vapor phases are flowing to pressure drop when gas or vapor only is flowing) versus the tube inlet Reynolds number and the vapor or gas specific volume. Data were obtained from isothermal test rigs in which nitrogen and liquid mercury flowed through glass tubes with and without swirl devices. Data were obtained from non-isothermal test rigs in which mercury was condensed by forced convection from quality of one to zero. Comparison is made with pressure drop data obtained from forced convection boilers in which mercury was evaporated from quality of zero to one. The effect of tube orientation on pressure drop is also discussed.

Conditions for maintaining a stable liquid column at the inlet of the condensate pump (subcooler) in zero gravity were experimentally investigated. This is referred to as interfacial stability. Both static and dynamic tests were made on mercury columns in glass and stainless steel tubes. Stability limits are defined.

Flow regime and flow regime stability were investigated by determining the critical gas velocity required to entrain mercury droplets. The effect of imposed body forces was evaluated. Measurements were taken under isothermal conditions using liquid mercury and nitrogen, and under non-isothermal, condensing conditions in zero gravity and in 2.55 gravity (WADD zero gravity flights). Primarily these tests provide the required critical Reynolds number for flow regime stability against external (body forces) disturbances.

The influence of non-condensable gas on flow performance in mercury forced convection condensers was experimentally observed both in zero gravity (WADD zero gravity flights) and in unity gravity. The danger to system performance of gas plugs in the subcooler lines was recognized and means of gas removal are suggested. Experimental efforts are under way.

TABLE OF CONTENTS

LIST OF FIGURES

LIST OF FIGURES (Continued)

1.0 INTRODUCTION

The SNAP II auxiliary power unit for 3 KW of electrical output consists of a reactor heat source and a power conversion system. The power conversion system is a mercury Rankine engine composed of a mercury boiler heated by a NaK heat transfer loop, an axial flow impulse turbine which extracts energy from the superheated mercury vapor, a condenser which returns the vapor to a liquid state and a mercury pump which returns the condensate to the boiler. The turbine directly drives the alternator, the mercury pump, and a permanent magnet induction NaK pump which is designed to circulate the NaK between the mercury boiler and the reactor.

Background information on mercury condensers was obtained from the SNAP I program. The lower power SNAP I system utilizes a similar mercury Rankine engine with an isotope heat source instead of a reactor. In the SNAP I system the low condenser pressure necessitated very low tolerable pressure drop which dictated very low vapor velocities in the condenser. The resulting large vapor flow area and the required small radiator area led to the concept of condensing between parallel plates over the entire radiating surface. This yields minimum radiator area, but weight is high.

Although the SNAP II condenser-radiator is a finned tube, the basic problems are the same as SNAP I problems. Basic investigations on fluid mechanics of two-phase flow, stability of the condenser-subcooler interface and identification of problems conducted during the SNAP I program have greatly aided the SNAP II condenser research effort.

2.0 REQUIREMENTS AND SPECIFICATIONS

The condenser of the SNAP II power conversion system condenses twenty pounds of mercury vapor per minute. The condensate is mixed with the liquid mercury discharged by the bearings. This total flow of forty pounds per minute is subcooled to 420°F and fed to the condensate pump inlet at 6 psia pressure. The condenser pressure drop requirement will be such that the overall system weight is minimized.

The condenser has the shape of a frustrum of a cone. It acts as a major structural member of the satellite vehicle, supporting the reactor and shield. Since the condenser essentially encloses the other components of the power conversion system, it must be capable of rejecting not only the condenser heat load, but also heat loading due to the losses of the other components. The losses reach the condenser surface by radiation from the individual components. The total vehicle skin area allotted to the condenser and subcooler as radiating surface is 110 square feet.

The mercury vapor passages in the condenser will be tubes attached to the vehicle skin which is the radiating surface. The number and size of the tubes should be selected to produce a minimum weight condenser which meets reliability and performance requirements.

The possibility of a power plant failure due to meteoric damage exists in space. Protection against meteoric penetration of the condenser tubes or other fluid-carrying lines in the system is partially supplied by the condenser radiating skin.

To minimize condenser weight and meteorite protection requirements a minimum number of tubes of a minimum size should be employed. To attain optimum system performance, however, the condenser pressure drop should be minimized with the requirement of large tubes. The condenser research program described in this report provides a designer with basic data to determine an optimum condenser design.

3.0 CONDENSER RESEARCH

To design a condenser in which liquid and vapor flow concurrently through the tubes, detailed information is needed about pressure drop, flow regime stability, and stability of the liquid-vapor interface.

When mercury condenses at 600°F, surface tension of the liquid is high and the volume ratio of vapor to liquid is large even though weight fractions of vapor to liquid are low. These factors produce a flow regime of liquid drops flowing with the vapor. To design a condenser with the maximum allowable pressure drop, and thus minimum weight, pressure drop associated with the flow of such a mixture must be accurately determined.

The stability of the flow regime affects both the pressure drop and the operation of the condenser. A stable flow regime is one in which no appreciable changes occur as a result of a change in body forces over the range expected. If body forces cause a change in liquid inventory in the condenser, an equal change occurs in subcooler inventory. The condenser, and consequently the entire system, then operates off design. Variation in liquid inventory in the condenser also causes a change in pressure drop through the condenser.

Another important factor in condenser design is the stability of the liquid-vapor interface which separates the subcooler from the condenser. It can readily be visualized that if a conventional earth-bound condenser were turned upside down, the liquid in the "hot well" would be dumped into the vapor inlet line which would cause the condensate pump to fail. Similarly, a glass of water when inverted will spill its contents, although a sufficient barometric pressure is available to support a 34-foot water column. Instability and wave formation at the interface between liquid and gas are the major factors breaking the liquid phase into drops and ligaments during spilling.

When a liquid interface is placed in a zero-gravity environment, it may be subject to gravity disturbances - plus or minus with respect to the interface. These disturbances are similar to those experienced when inverting a container with a liquid interface. If the proper disturbing wavelength is imposed on the interface, an instability may cause the liquid to "spill". This must be avoided in a zero-gravity environment. A fixed column of liquid properly subcooled for the required net positive suction head is necessary for good performance of the power plant system.

The following sections describe in detail efforts and results in research devoted to problems of interfacial stability, flow regime, and pressure drop during the SNAP II condenser development program.

3.1 Interfacial Stability

Experiments were conducted to establish parameters needed to maintain a stable liquid column in the subcooler and inlet to the pump in the presence of various

disturbances. These investigations were divided into two areas: static stability and stability with external disturbances.

3.1.1 Static Interfacial Stability

In a gravitational field the interface between two fluids of different densities is stable if the heavier fluid is at the bottom. For example, the liquid surface in a pan of water at rest on the surface of the earth is certainly stable; similarly, a condenser tube on the surface of the earth in which flow is vertically downward will have a stable liquid-vapor interface at the bottom of the tube.

Theoretically, an interface is stable if no body forces are present. However, in space where no body forces are present, very small disturbances could cause interfacial instability. A condenser operating in space is expected to experience some disturbances due to turbomachinery vibrations, two-phase flow turbulence and meteoric impacts. If any of these disturbances causes the interface to become unstable and break, liquid will be thrown from the subcooler into the condenser. This will increase the condenser area and decrease the subcooler area. If enough liquid is taken from the subcooler, vapor may enter the pump and cause stoppage of the flow and a consequent shut-down of the power conversion system.

Texts such as Hydrodynamics by Lamb and Theoretical Hydrodynamics by Milne-Thompson have discussed interfacial stability. If two fluids at rest and of different density are superposed, wave motions can take place on the interface between them. The velocity is given by:

$$C = \sqrt{\frac{g\lambda}{2\pi}\,\frac{(\rho_1 - \rho_2)}{(\rho_1 + \rho_2)} + \frac{2\pi\sigma}{\lambda(\rho_1 + \rho_2)}} \qquad (1)$$

where ρ_2 is the upper fluid density
g is the gravity acceleration
σ is surface tension
λ is wave length
ρ_1 is the lower fluid density

The condition for stability is that the velocity C is real, which is always satisfied if ρ_2 is less than ρ_1, corresponding to the pan of water on the surface of the earth. The equation is of interest when ρ_2 is greater than ρ_1 and C is real, which is satisfied if

$$\lambda \leq 2\pi\sqrt{\frac{\sigma}{(\rho_2 - \rho_1)g}}$$

An interface between two parallel vertical plates is stable if the spacing between the plates is less than $\frac{\lambda}{2}$, as discussed by Lamb. The maximum spacing, δ, for a stable interface between liquid mercury and mercury vapor is given by:

$$\delta_{max} \cong \pi\sqrt{\frac{\sigma}{\rho_\ell g}} \quad \text{if} \quad \rho_\ell >> \rho_g$$

for $g = 32.2$ ft/sec^2, $\delta_{max} = 0.233$ inch.

For the three-dimensional case of mercury in a tube, the maximum diameter for stability is expected to be the same order of magnitude as for the two-dimensional case of parallel walls. Placing liquid mercury in glass tubes of various diameters and inverting the tubes showed that an inverted tube will have a stable interface if the tube diameter is less than 0.157 inch.

Interfacial stability tests were first performed at room temperature using four straight pyrex glass tubes 0.1696, 0.1797, 0.1908 and 0.209 inch in diameter respectively and two tapered tubes. The straight tubes were sealed at one end and filled with a short column of mercury. The tubes were then inverted, both slowly and also with a sudden movement. Only the smallest of the four straight tubes would hold a column of mercury and this tube did not hold consistently, indicating that the critical tube diameter should be just under 0.1696. This diameter was marked on the tapered tube as a guide. The tapered tube was then filled with mercury to a diameter somewhat smaller than 0.1696 and small increments of mercury were added until the column would just support itself in the tube, i.e., the addition of just one more drop of mercury would cause the column to spill or break loose from the tube, as shown in Figure 1. The diameter was then measured by dropping precision dowel pins into the tapered tube. The diameter was 0.157 inch.

Repeated tests showed that moisture or any foreign matter on the inner wall of the tube prevented reproducibility of test results. The critical diameter of 0.157 inch was observed consistently during several tests on both tapered tubes when they were clean and dry. However, after the tubes had been heated, with the consequent formation of moisture, the mercury column would not support itself. After the tapered tubes had been cleaned and thoroughly dryed, the critical diameter was again obtained.

These tests were repeated in Type 316 stainless steel tubes. To obtain a range of inside diameters, holes were drilled and reamed in bar stock. The tubes were cleaned with alcohol and dried. The following diameters were

INTERFACIAL STABILITY IN TAPERED GLASS TUBE

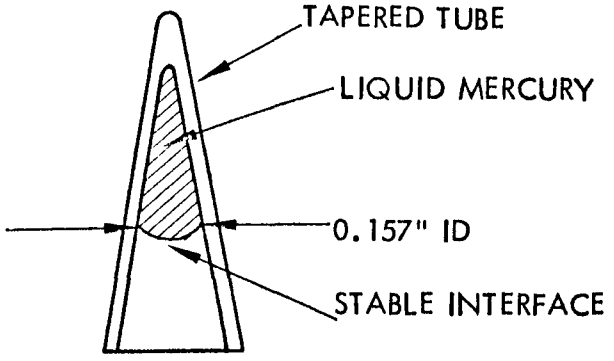

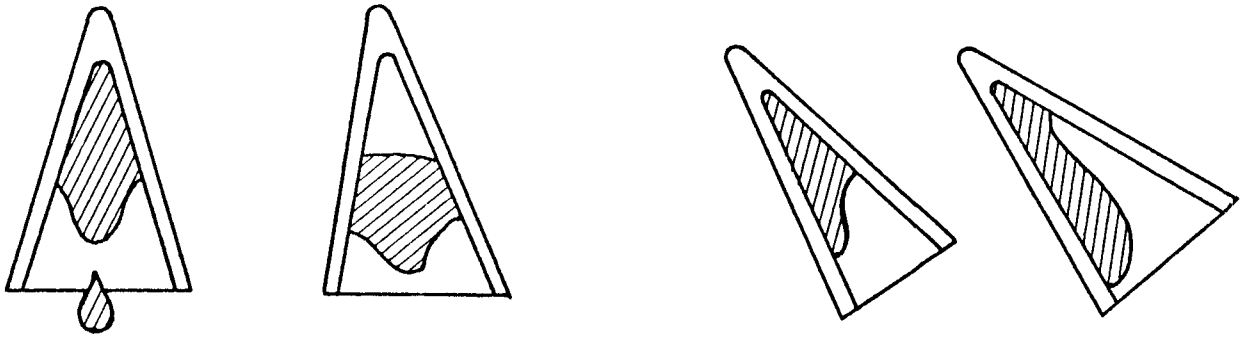

TUBE INVERTED RAPIDLY

TUBE INVERTED SLOWLY

UNSTABLE DIAMETERS

RESULT OF HAVING TOO MUCH MERCURY IN TUBE

FIGURE 1

tested: 0.118, 0.133, 0.140, 0.149, 0.158, 0.165, 0.168, 0.176, and 0.180 inch. The largest tube which held a stable interface was the 0.168 inch diameter tube. Behavior similar to that observed in the glass tubes was observed with the 0.168 inch diameter tube, i.e., the tube had to be thoroughly clean and dry or the mercury would not hold in the tube.

To determine the effect of temperature on the critical diameter, the five largest stable steel tubes were filled with mercury and placed inverted in glass test tubes containing a few drops of mercury. The mercury in the test tube was to provide a mercury vapor atmosphere in contact with the interface. The five test tubes containing the inverted mercury-filled tubes were then placed in a small oven and the temperature was slowly increased. Thermocouples welded to the outside of the tubes indicated the tube temperature. Figure 2 is a schematic of the test apparatus.

As the temperature was increased, the mercury dropped out of the tubes. Sometimes all the liquid spilled at once, while at other times it slowly dripped out. When the mercury spilled, the tube temperature was recorded. The test procedure was repeated nine times. The first few test results showed no definite trend in temperature versus tube diameter. Erratic results were believed to be caused by air entrapped in the mercury which expanded on heating and pushed the mercury out of the tube and by the possibility of contamination of the tubes.

After every test the tubes were cleaned and dried, filled with mercury, placed in a vacuum chamber and gently tapped to remove the air which was trapped in the tube. The tubes apparently became cleaner and the degassing technique improved with each test. In the last three tests, all five of the mercury columns spilled when the tube temperature reached 672°F, which is the mercury boiling point at atmosphere pressure.

Before interfacial stability can be considered, the mercury vapor pressure must be less than pressure at the interface. This condition was present in the inclined condenser tests discussed in Section 3.3 of this report. Apparently the mercury drops which originate on the condenser wall are subcooled before reaching the interface. Subcooling is also caused by conduction of heat back through the liquid and by surface tension which increases pressure at the interface.

The maximum stable diameter of 0.168 inch holds only for the particular tube material and surface finish tested. The reamed hole in the Type 316 stainless steel tube had a surface finish measured as 40 microinches rms. The effect of materials is evident in a comparison with the pyrex glass tube where the critical diameter was 0.157 inch. The effect of surface finish was observed by attempting to hold mercury in a Type 316 stainless

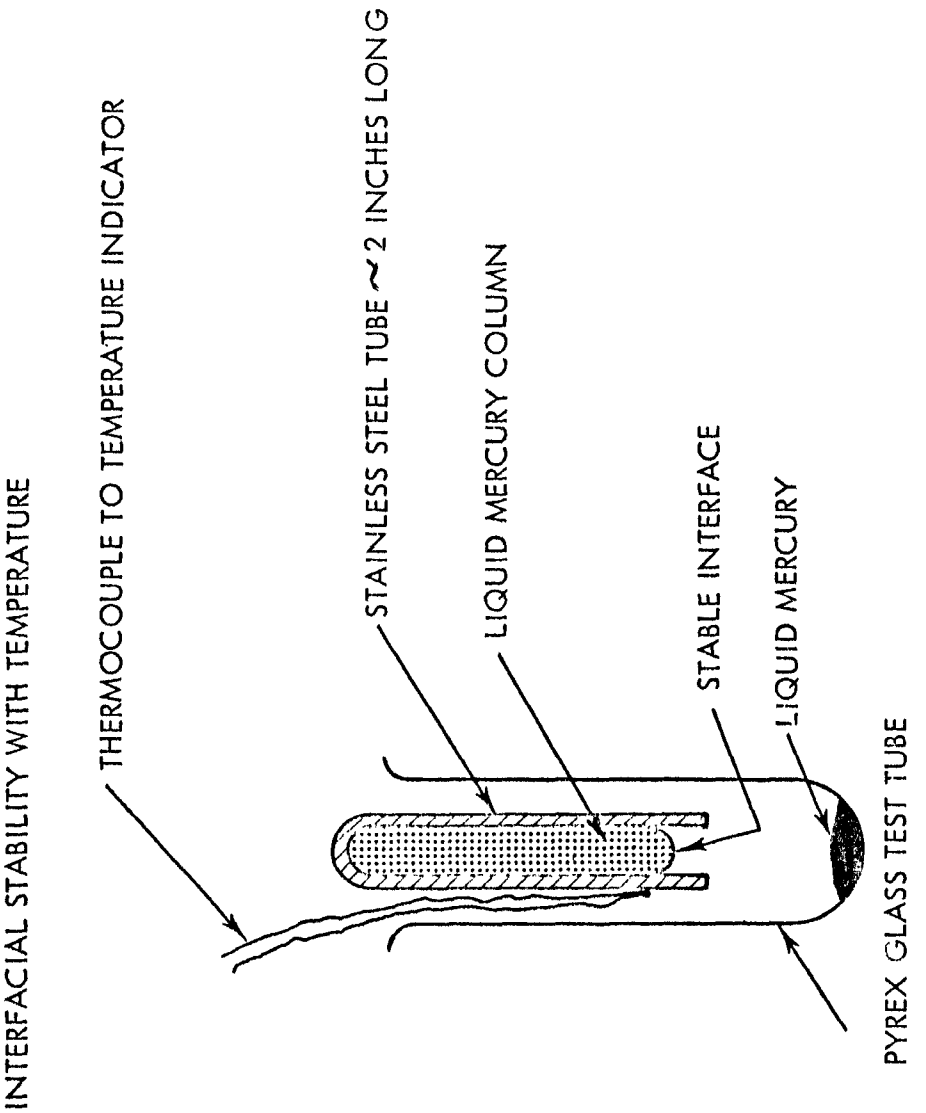
INTERFACIAL STABILITY WITH TEMPERATURE
THERMOCOUPLE TO TEMPERATURE INDICATOR
STAINLESS STEEL TUBE ~ 2 INCHES LONG
LIQUID MERCURY COLUMN
STABLE INTERFACE
LIQUID MERCURY
PYREX GLASS TEST TUBE

FIGURE 2

steel tube of 0.133 inch inside diameter which had been vapor blasted.

The tube could not hold a mercury column when inverted. The inside surface was measured at 65 microinches rms. This indicates that the inside of a condenser tube should be smooth in the vicinity of the interface. Specifying an rms value for the tube may not be sufficient, because the finishing process may also have an effect.

3.1.2 Interfacial Stability with External Disturbance

The previous section shows that static stability can be guaranteed against small disturbance by proper choice of tube diameter at the interface. However, since forced vibrations on a statically stable interface could cause the interface to break, tests were conducted to determine interfacial stability with external disturbances.

In these tests, mercury in a glass tube was subjected to vibrations of various frequencies and amplitudes and the boundaries of instability were noted. The results of the tests are shown in Figure 3. As expected, the test points define a hyperbolic type curve which indicates that at very low frequencies the interface is stable to all amplitudes and at very low amplitudes the interface is stable to all frequencies. Sketches indicating the appearance of the interface when unstable and stable are also shown in Figure 3. The surface had the appearance of a "cow's udder" in which the "teats" broke off into drops and formed a spray. At high amplitudes a single "teat" was observed which broke off into a single drop. From observations of the disturbed interface it was concluded that a vibrating membrane described in texts on vibration behaves in a similar manner. The nodal circles and nodal diameters referred to in these texts apparently are similar in appearance to the disturbed interface noted in Figure 3. These tests were conducted on an "M.B." Shaker in horizontal glass tubes. Displacement was vertical. The glass tube was rigidly mounted on the shake table to minimize secondary vibrations.

If the power conversion system is required to operate in the presence of relatively large disturbances, a map of these disturbances can be superposed on Figure 3 and the proper tube size can be chosen so that no vibrations lie in the unstable region. For more accurate predictions of stability limits with external disturbances, the tests described should be repeated with mercury in steel tubes and at 600°F in order to duplicate as closely as possible actual condenser conditions. This would be important if the condenser were required to operate under vehicle launch conditions where vibrations may be appreciable. However, at present an orbital start is planned and vibrations of the magnitude shown in Figure 3 seem unlikely. Therefore no refinement of the stability limits with external disturbances is deemed necessary.

STABILITY WITH EXTERNAL DISTURBANCES

LIQUID MERCURY IN HORIZONTAL GLASS TUBES, VERTICAL DISPLACEMENT

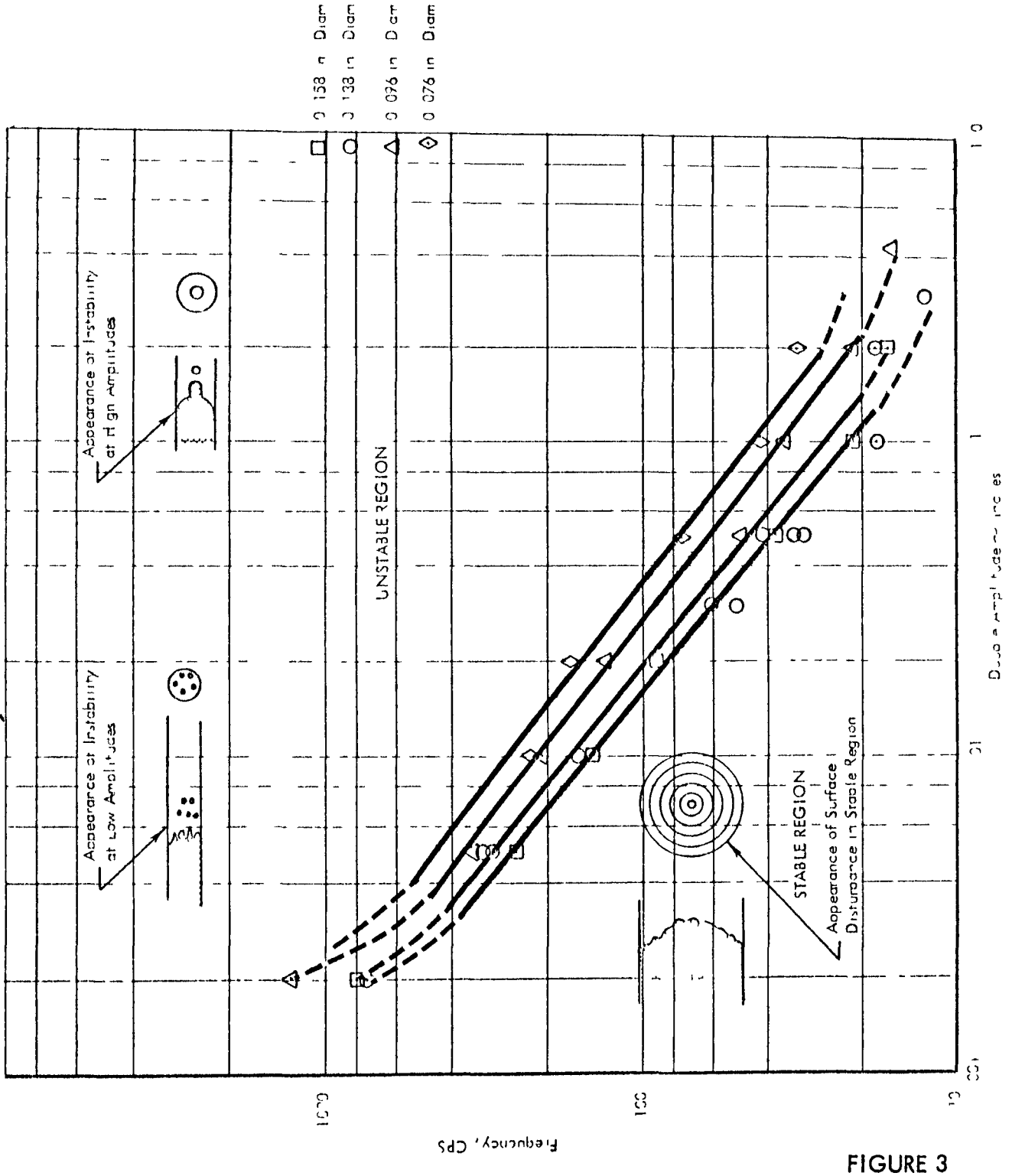

FIGURE 3

3.2 Two-Phase Flow Investigations

Since in an orbiting vehicle a net body force is absent, the only method of moving condensate from the condenser to the subcooler is by means of the drag forces exerted on the liquid by the flowing vapor. It is therefore necessary to understand the fluid mechanics of a liquid and vapor mixture flowing in a passage, i.e., "two-phase flow." Not only must the phenomena be understood for design purposes, but in the final design the flow must be stable and predictable so that small disturbances or off-design operation will not drastically change the performance of components directly affected by condenser performance, namely the turbine and condensate pump. Many experimenters have been investigating the fluid mechanics of two-phase flow, but to date no general correlation is available. Therefore it was desirable to visually observe the two-phase flow of mercury and to obtain pressure drop predictions for a mercury condenser.

3.2.1 Two-Phase Flow Tests

To obtain two-phase flow pressure drop data without the complications of heat transfer and condensing, two-phase flow tests were conducted using nitrogen gas and liquid mercury flowing through a transparent glass test section. Figure 4 is a photograph of the test apparatus.

In operation, dry nitrogen gas is metered and mixed with liquid mercury and ducted to a glass test section four feet long. Pressure drop was indicated on a mercury manometer connected to static pressure taps at each end of the test section.

The two-phase mixture leaving the test section enters a separator where the nitrogen is vented and the liquid is collected and weighed. Valves control the nitrogen and mercury flow into the mixing tee. The test section had an inside diameter of 0.394 inch and all tests were run with the test section in the horizontal position. Quick-closing pneumatically operated valves were located at the inlet and exit of the test section. By closing these valves simultaneously, the liquid mercury was trapped in the test section and could be removed and weighed to determine the liquid inventory.

The most striking phenomenon observed in these two-phase flow tests was the fact that when a mixture of liquid mercury and nitrogen gas entered a pipe line, the tendency was towards separation of the two well-mixed phases. This phenomenon was observed by a number of two-phase flow investigators using water and air, but in the case of liquid mercury an additional phenomenon, peculiar to mercury only, was noted: as the gas flowed rapidly down the tube, the liquid mercury was left behind in drop form, being moved slowly (relative to the gas) by the drag of

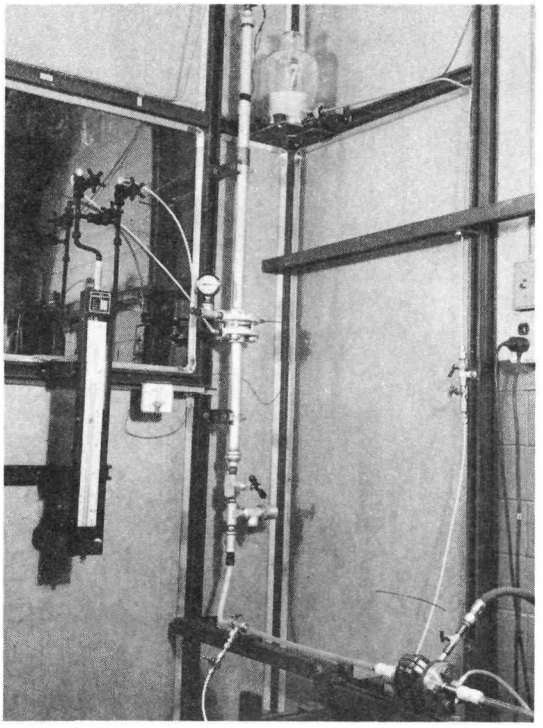

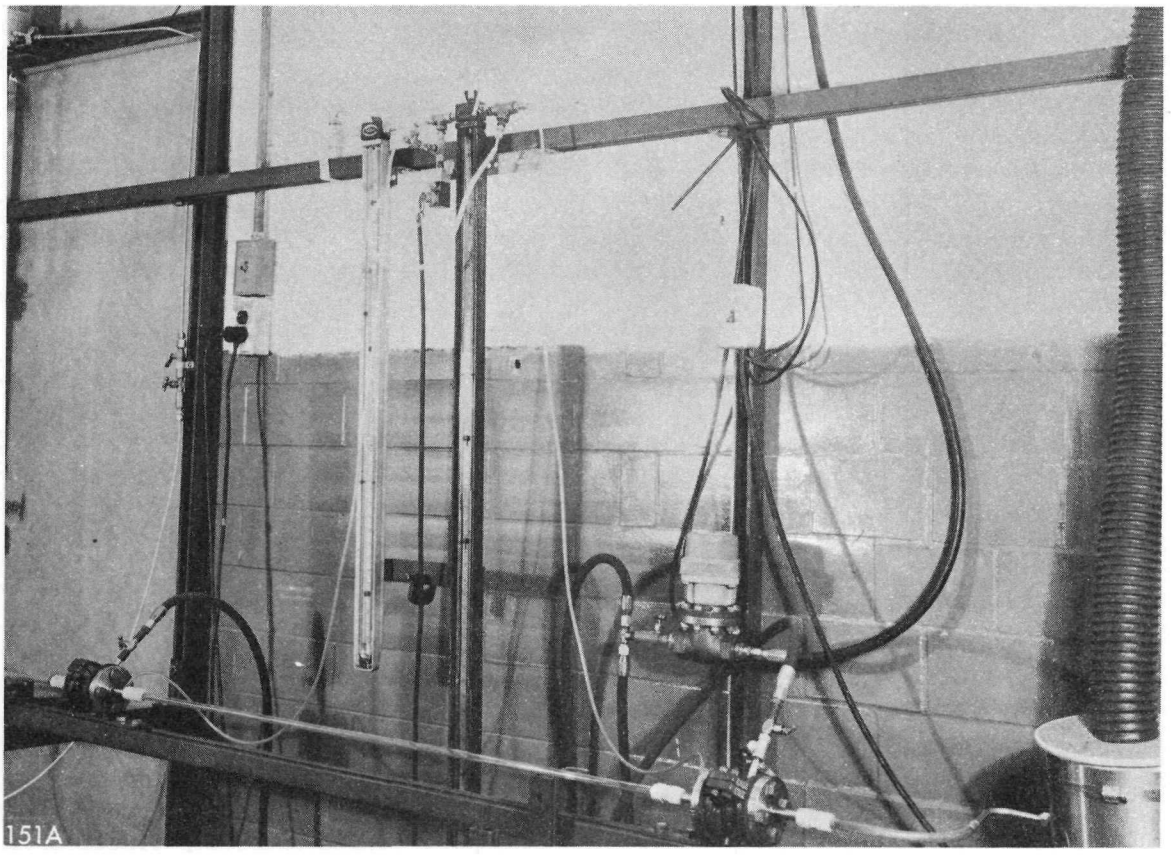

TWO PHASE FLOW RIG

FIGURE 4

the gas on the drops. Since the gas phase was moving two to twenty times faster than the liquid phase, the droplets had a tendency to slow down and to accumulate in the tube. For "equilibrium" conditions, the liquid drops would have to leave the test section at the same velocity as they entered it. Equilibrium conditions were not reached because the available tube length was not sufficient. Since such an "equilibrium" condition does not exist in an actual condenser, no special effort was made to achieve such fully developed flows. Due to the non-wetting properties of liquid mercury, it was impossible to obtain a continuous liquid film or layer of mercury. The liquid phase was always in drop form of one sort or another.

The following patterns were observed with the concurrent flow of nitrogen and liquid mercury (non-wetting) and are sketched in Figure 5:

a. Caterpillar Flow - The liquid phase is never continuous; it is broken into long, caterpillar-like drops which are equally spaced and move at the same velocity.

b. Drop Flow - The caterpillars are broken into smaller drops by the higher gas flow. Again the spacing between drops is fairly even and only little drop growth is noticed.

c. Turbulent Flow - The high gas rate causes turbulent movement of the drops. The drops bounce off the walls, colliding with each other and growing in size.

d. Semi-Annular Flow - The small drops on the bottom are moving very rapidly and closely together (to the naked eye, there seems to be a continuous liquid stream). Smaller drops are moving along the walls with some drops dispersed in the gas stream.

e. Fog Flow - The drops are picked up from the walls by the very fast-moving gas and dispersed in the gas stream. The drops are so small that they cannot be seen by the unaided eye.

In addition to these main flow patterns, a few transition patterns were noted. For instance, if in turbulent flow the liquid rate was increased, the flow pattern seemed to approach the wavy pattern of wetting fluids, but we cannot define such a pattern, because no continuous liquid phase was ever observed with liquid mercury. The fast-moving large drops, being in a highly turbulent state, only appear to form a continuous layer of mercury. The transition between semi-annular flow and fog flow is very sudden. No annular flow, in the strict sense of the word, was ever observed. The drops on the bottom of the tube were always larger and more numerous than the drops along the walls of the tube. This is a gravity phenomenon which will

OBSERVED TWO-PHASE FLOW REGIMES FOR
LIQUID MERCURY AND NITROGEN GAS
IN A HORIZONTAL TUBE

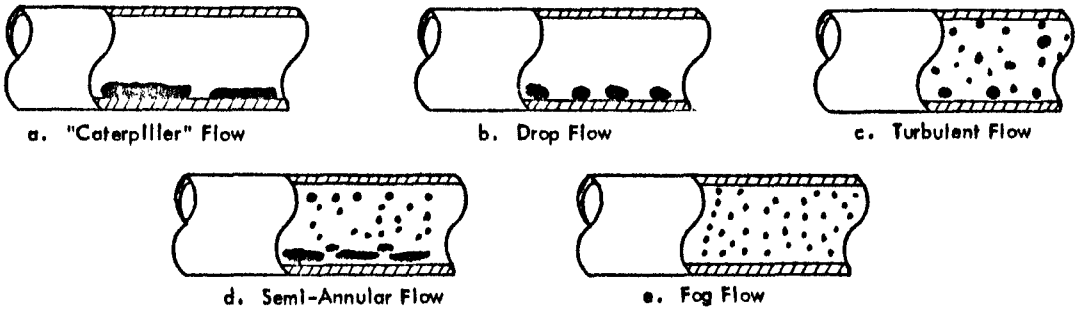

FIGURE 5

be discussed in detail later.

Figure 6 is a two-phase flow map in which the variables are the liquid and gas weight flow rates. The transition between the flow patterns cannot be pin pointed and for this reason, areas rather than lines were drawn as demarcation between the different zones. It may be noted that at high liquid and low gas rates, an unsteady and slugging type of flow exists. The flow map points out one important factor, namely, that for a given tube configuration and orientation, the flow patterns are functions of the two weight flows only.

3.2.1.1 Pressure Drop

The pressure drop in any two-phase flow system is greater than that for the flow of either phase flowing alone. This increase in pressure drop is due to the shear forces on the walls, the drag forces due to the particles, and the fact that the presence of the second fluid reduces the cross sectional area of flow for the first fluid.

In presenting two-phase flow pressure drop data, it is customary to plot the pressure drop ratio versus the flowing quality. The pressure drop ratio is the ratio of the two-phase pressure drop ΔP_{TP} to the pressure drop due to the gas alone, ΔP_g. The following quality is defined as the ratio of the flow rate of the gas to the total flow. The reduced test data are presented in tabular form in Appendix II.

Figure 7 is such a plot for the nitrogen-liquid mercury data. The pressure drop ratio is seen to be greatly influenced by the gas flow rates. An increase in mercury flow (decrease in quality) also increases the pressure drop ratio, but to a much lesser extent. We can conclude that the pressure drop is most sensitive to the gas flow.

A comparison of the pressure drop data with the well-known Martinelli correlation is in order. Figure 8 shows this comparison for the case of viscous-turbulent flow which Martinelli defines as the gas Reynolds number greater than 2000 and the liquid Reynolds number less than 1000. The spread in data is no greater than the spread in Martinelli's data used to obtain the curve. It is also evident that the spread is not random but that ϕ_{gvt} increases with gas flow rate. As will be shown later, there is evidence that this may be gravity phenomenon and could be a result of the type of test apparatus used to obtain the data.

Two-phase flow pressure drop data are useful to predict pressure

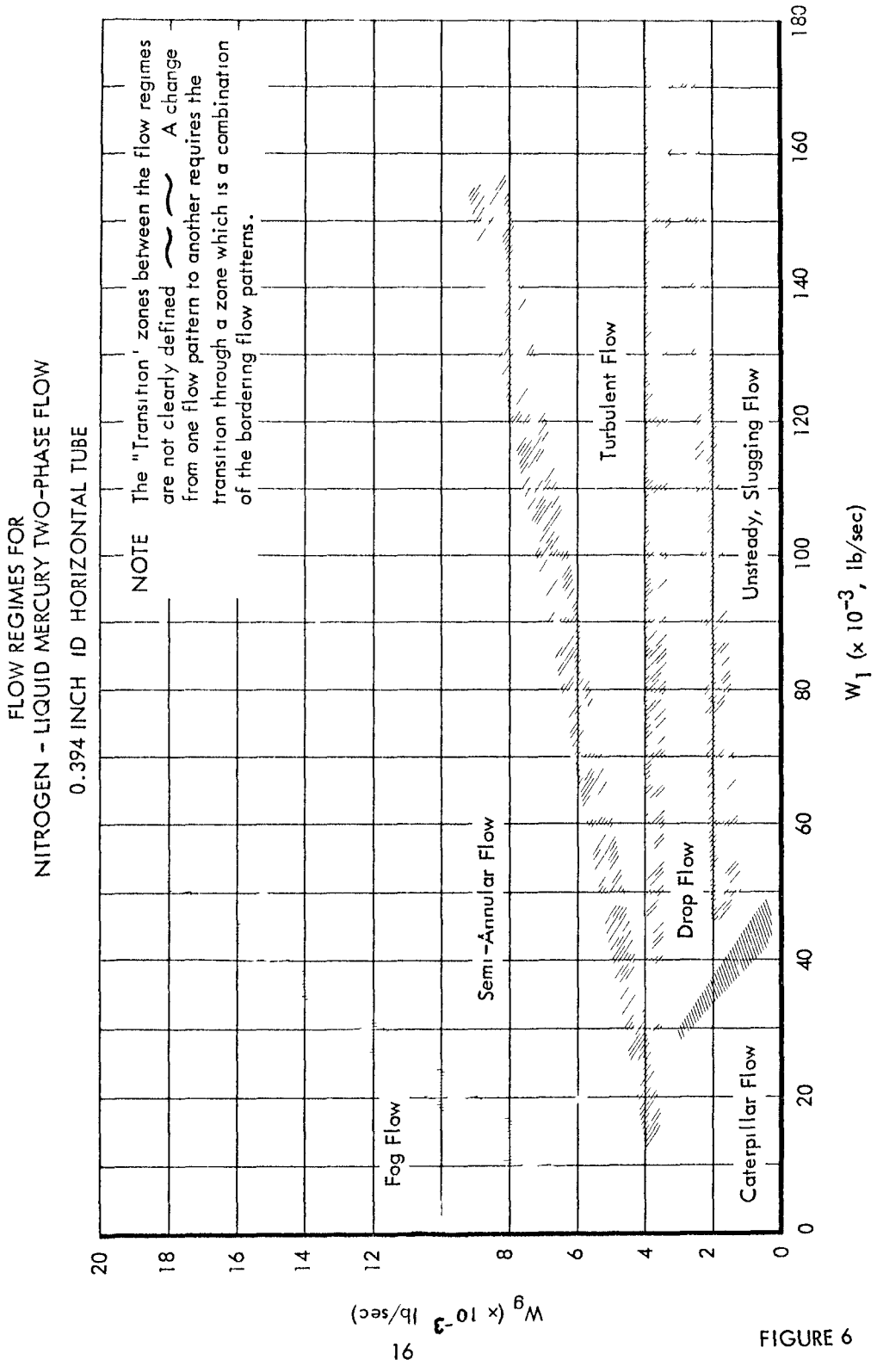
FLOW REGIMES FOR
NITROGEN - LIQUID MERCURY TWO-PHASE FLOW
0.394 INCH ID HORIZONTAL TUBE
NOTE The "Transition" zones between the flow regimes are not clearly defined ~~~ A change from one flow pattern to another requires the transition through a zone which is a combination of the bordering flow patterns.
Fog Flow
Semi-Annular Flow
Drop Flow
Caterpillar Flow
Turbulent Flow
Unsteady, Slugging Flow
W_g (x 10^{-3} lb/sec)
W_l (x 10^{-3}, lb/sec)
0
2
4
6
8
12
14
16
18
20
0
20
40
60
80
100
120
140
160
180

FIGURE 6

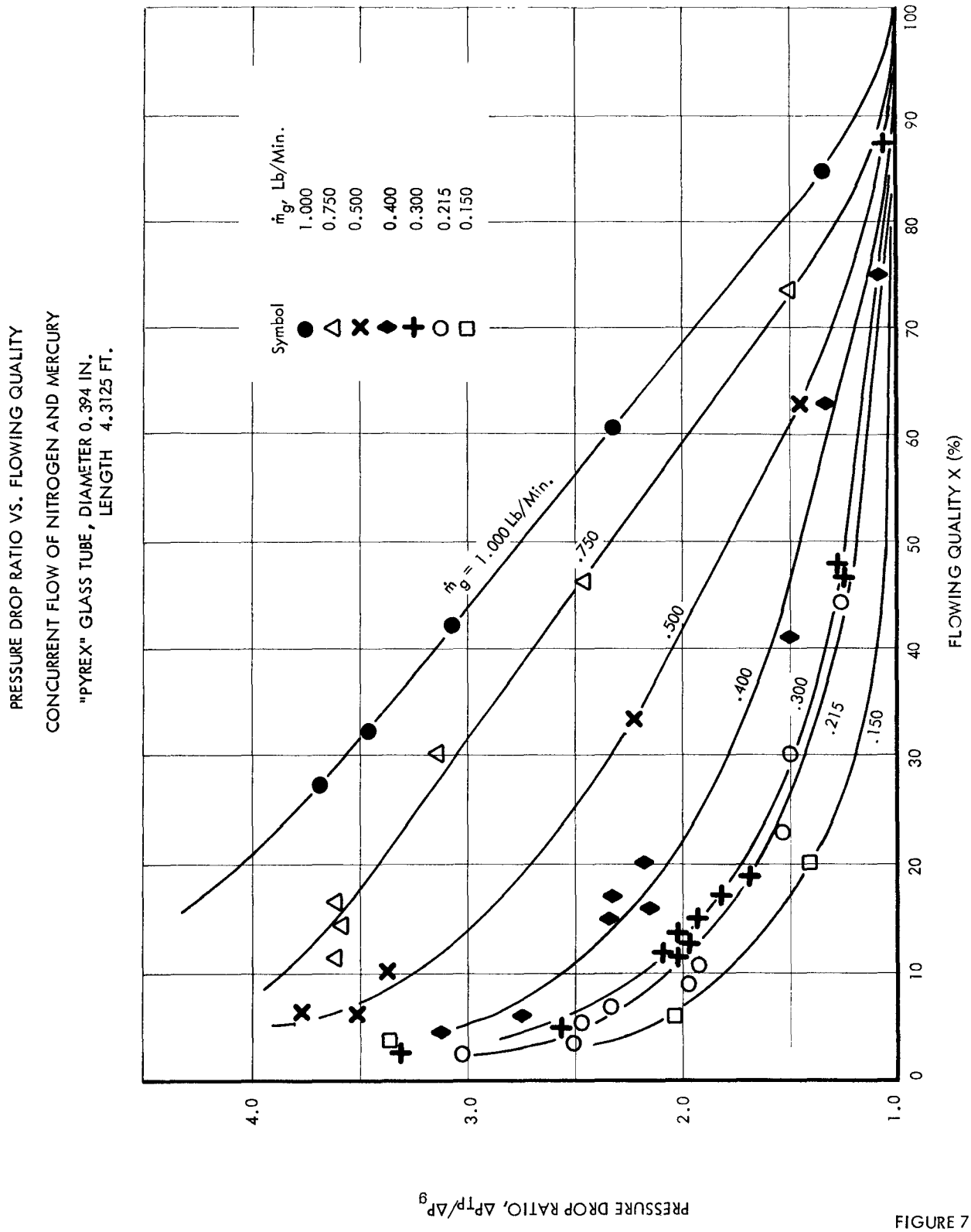
PRESSURE DROP RATIO VS. FLOWING QUALITY
CONCURRENT FLOW OF NITROGEN AND MERCURY
"PYREX" GLASS TUBE, DIAMETER 0.394 IN.
LENGTH 4.3125 FT.
Symbol
$\dot{m}_g$, Lb/Min.
1.000
0.750
0.500
0.400
0.300
0.215
0.150
$\dot{m}_g$ = 1.000 Lb/Min.
.750
.500
.400
.300
.215
.150
PRESSURE DROP RATIO, $\Delta P_{TP}/\Delta P_g$
FLOWING QUALITY X (%)
4.0
3.0
2.0
1.0
0
10
20
30
40
50
60
70
80
90
100

FIGURE 7

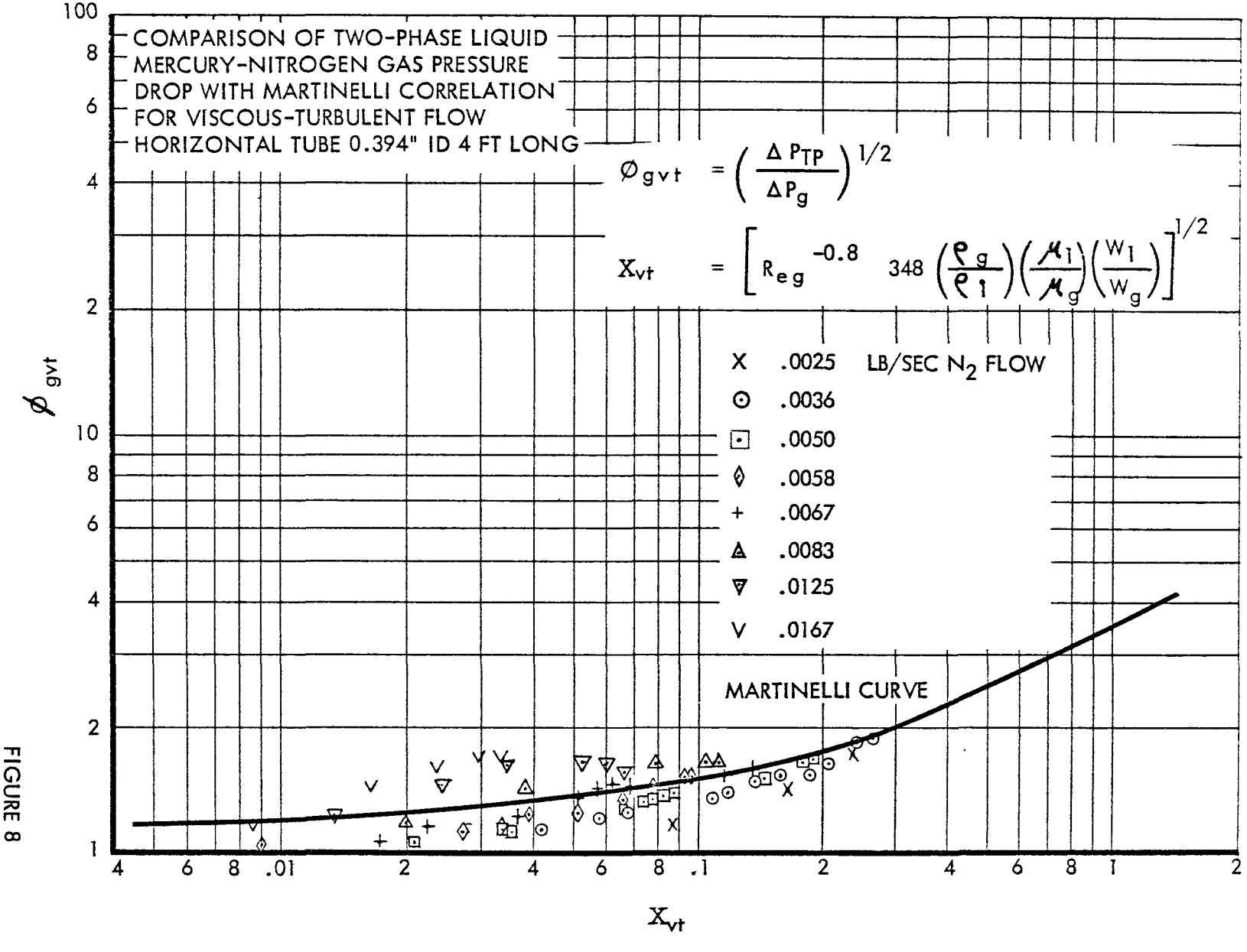

FIGURE 8

drop in a condenser. However the results of such a procedure are to be considered approximate since different mechanisms are involved in the flow. In the two-phase flow test rig, liquid mercury is atomized in the flowing nitrogen and the mixture flows through the test section. In the condenser vapor enters the inlet and condensation occurs along the tube. The liquid drops grow on the surface until they are swept away by the flowing vapor. The mass flow rate of vapor is decreasing while the flow rate of liquid is increasing along the length of the condenser tube. Therefore any one data point taken in the two-phase flow test rig represents one point in the condenser. To use this data to predict condenser pressure drop, the data from curves such as Figure 7 must be integrated to obtain the pressure drop in condensing a vapor from a quality of unity ro zero.

3.2.1.2 Hold-Up

The liquid hold-up in a system is important from the viewpoint of inventory considerations. For every nitrogen-liquid mercury test run, the liquid hold-up was obtained by the quick-closing valve technique.

Figure 9 shows the liquid hold-up (defined as the volume fraction of liquid in the test section) as a function of the flowing quality. On the same graph are plotted theoretical relationships and semi-empirical correlations for comparative reasons. The test points fall between the theoretical fog flow equation and the Martinelli liquid hold-up correlation. This indicates that although fog flow was approached, it was never reached. Fog flow can be achieved only with very small drops which travel at the same velocity as the gas. The deviation from the Martinelli curve is due to the fact that the Martinelli model is based on continuous liquid and gas phases, whereas in the case of a non-wetting fluid, the liquid phase is discontinuous (drop flow of one kind or another) and only the gas phase is continuous. This means that the volume occupied by the liquid is appreciably smaller in the non-wetting case, and thus the experimental liquid hold-up is less than predicted by Martinelli's curve.

Figure 9 shows that the experimental results follow the trend of the fog-flow curve but are approximately ten times as large. An approximation of the condenser inventory can be made assuming that the liquid volume fraction will be ten times that for the fog flow case.

LIQUID HOLD-UP
TWO-PHASE FLOW TEST RESULTS
LIQUID MERCURY - NITROGEN GAS
HORIZONTAL 0.394 INCH I.D. TUBE - 4 FEET LONG

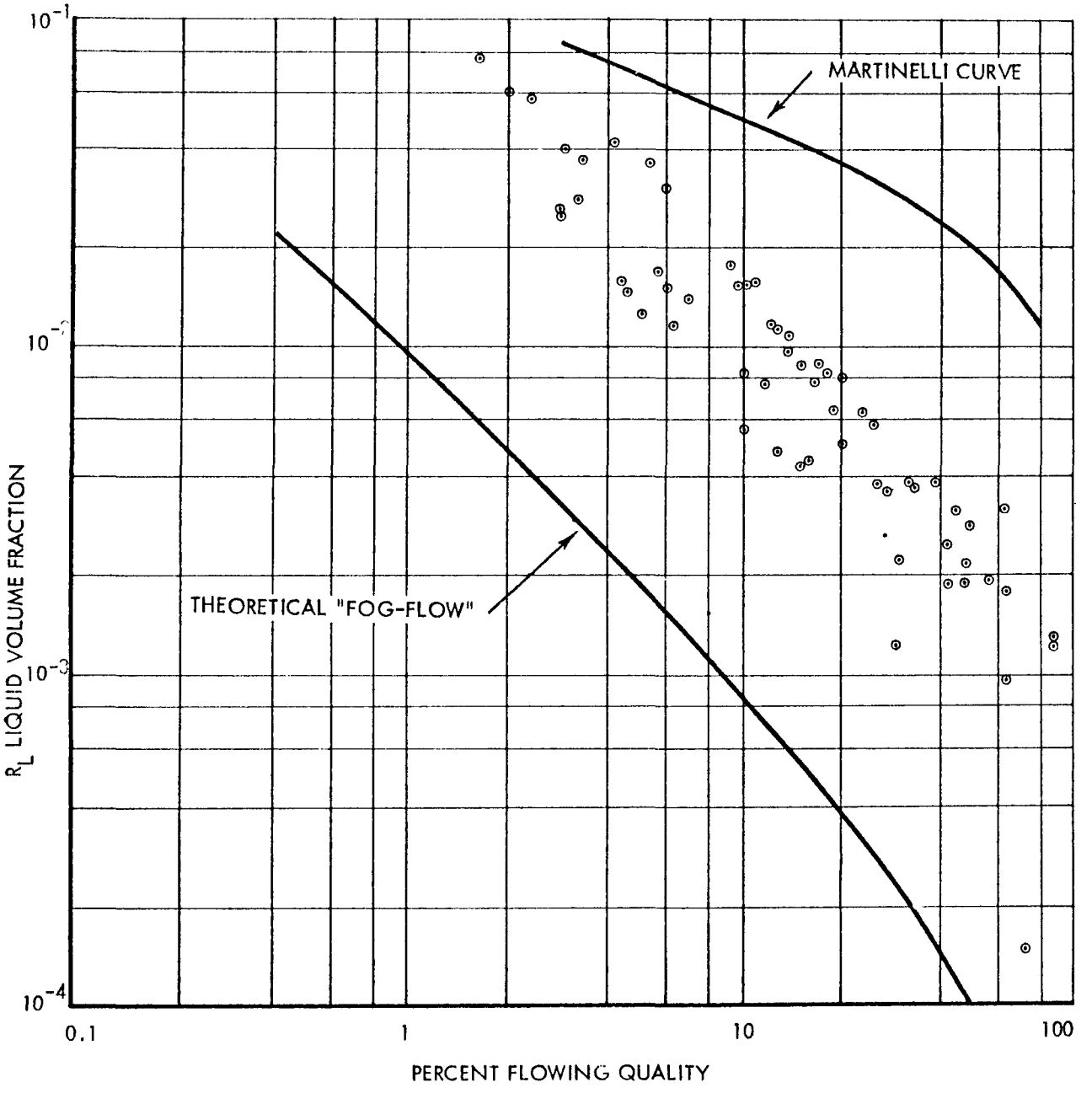

FIGURE 9

For fog flow the liquid and vapor have the same velocity and therefore the weight of liquid will be equal to the weight of vapor in the tube. Since the volume fraction of liquid is small it can be neglected in computing the vapor volume in the tube. Therefore the liquid weight in the tube will be ten times the vapor weight and the total weight of mixture in the condenser tube will be eleven times the weight of vapor which can be contained in the tube volume.

3.2.1.3 Flow Regime Stability

The flow pattern for a two-phase flow system is determined by conduit shape, body or gravitational forces, interphase forces (normal and shear stresses), and intraphase forces (surface tension). In general the flow patterns can be classified as (1) gas phase dispersed in a continuous liquid phase (bubbles), (2) liquid phase dispersed in a continuous gas phase (droplets or fog), (3) both phases continuous with wavy or smooth interface. The high surface tension (intraphase force) of non-wetting liquid mercury and the mercury vapor drag force (interphase force) exerted by the flowing vapor on the liquid mercury tends toward a flow regime of liquid mercury droplets dispersed in vapor. This general flow pattern can be further classified as to the size of the mercury droplets.

Pressure drop and inventory data can be correlated only if the flow pattern is defined. For example, the pressure drop in a pipe can be computed if it is known whether the flow is laminar or turbulent. In the design of a zero-gravity condenser the characteristics of the two-phase flow system must be such as to be independent of any body forces that may be imposed during launch, ground testing, or in orbit. At zero gravity it is anticipated that some body force disturbances may occur. If the condenser flow pattern is sensitive to body forces, then the resulting alteration in flow pattern will cause changes in condenser liquid hold-up which in turn causes a shift in the position of the subcooler - condenser interface and changes in the amount of subcooling. Since the two-phase pressure drop also depends on flow pattern, a change in pressure drop will occur with imposed body force disturbances. Tests have indicated this to be true. At low Reynolds numbers the condenser pressure drop measurements will be shown to be sensitive to inclination. At the higher Reynolds numbers the differences disappeared, indicating that the flow pattern is no longer dependent on the Froude number (ratio of inertia to gravity forces).

Tests have been made in zero gravity and in the laboratory to determine the minimum design Reynolds number at which two-phase

flow is independent of gravity. The following tests provided the necessary information:

1. Critical Drop Size Measurements - A determination of the relationship between gas flow and drop size at instant of entrainment.

2. Zero-Gravity Tests - Visual indication of flow regime sensitivity to gravity.

3. Pressure Drop Measurements in Mercury Condensers - Dependence of pressure drop on gravity.

Measurements of Critical Droplet Size

The most difficult flow phenomenon to analyze is that involving the motion of a dispersed substance within a flowing fluid. The dispersed substance might be solid particles, liquid droplets, gas bubbles, or immiscible droplets. The number of variables required for rigorous analysis is usually too great to be handled experimentally or analytically. As a result, the problem is to simplify without significantly detracting from the physics of the phenomenon. For a two-phase flow system the same variables as for a single-phase fluid are used (Reynolds, Weber, Froude, Mach., etc.) in addition to the ratio of the properties of the dispersed substance to the continuous fluid (viscosity, density, etc.). In the majority of cases the following minimum number of variables should be considered:

1. A boundary scale term such as the pipe diameter.

2. A velocity to define the kinematics of the main flow.

3. The properties of the main flow, such as density and viscosity.

4. The dispersed phase described by a linear dimension (diameter if spherical droplets); specific weight if the effect of gravity on the flow is to be investigated; density; viscosity; surface tension of liquid-vapor interface; and the concentration.

A function as follows will result:

$$f\,(D, U_g, \mu_g, \mu_\ell, \rho_g, \rho_\ell, \gamma, d, \sigma, C) = 0 \qquad (2)$$

or in terms of dimensionless parameters Equation 2 may be expressed as:

$$f\left(\frac{D\rho_g U_g}{\mu_g}, \frac{\rho U_g^2}{\gamma d}, \frac{d\rho_g U_g^2}{\sigma}, \frac{d}{D}, \frac{\mu_g}{\mu_\ell}, \frac{\rho_g}{\rho_\ell} \frac{C_f}{C_w}\right) = 0 \text{ ----- } (2)$$

f(Reynolds No., Froude No., Weber No., d/D, μ_g/μ_ℓ, ρ_g/ρ_ℓ C/Cw) = 0

where
- D - tube diameter, ft
- U_g - gas velocity, ft/sec
- ρ_g - gas density, lbm/ft^3
- ρ_ℓ - liquid density, lbm/ft^3
- γ - specific weight due to gravity, lbf/ft^3; $\gamma = \rho_g$
- σ - surface tension, lbf/ft
- C - concentration (number of droplets per unit volume)
- C_w - Concentration on wall
- C_f - Concentration in flowing gas
- μ_g - gas viscosity
- μ_f - liquid viscosity

If certain characteristics of the droplets are determined by the flow, flow becomes the dependent variable. For the case investigated the droplet size was determined by the gas velocity. For the tests under consideration the number of droplets in the tube was held to a minimum; therefore, droplet interference was minimized, and C in Equation 2 was eliminated as a variable.

In the tests mercury droplets were sprayed onto the inside surface of a glass tube. The droplets were then measured by cross-hair in a microscope. The nitrogen flow rate required to pickup or entrain the droplet into the gas stream was then determined. Figure 10 shows a schematic of the test. This test simulated the conditions in a mercury condenser in which drops grow on the surface by condensation until they are large enough to be entrained by the flowing vapor. If by chance another drop would collide with the droplet in the view of the microscope, the data would not be recorded since entrainment was caused by collision and not by the gas. This phenomenon was rare. During the tests ρ_g was not varied by much, and since ρ_f was constant, the property ratio ρ_g/ρ_f, was not a major variable. Surface tension and the property ratio μ_g/μ_ℓ were also constant.

SCHEMATIC OF TEST
TO DETERMINE CRITICAL MERCURY
DROP SIZE

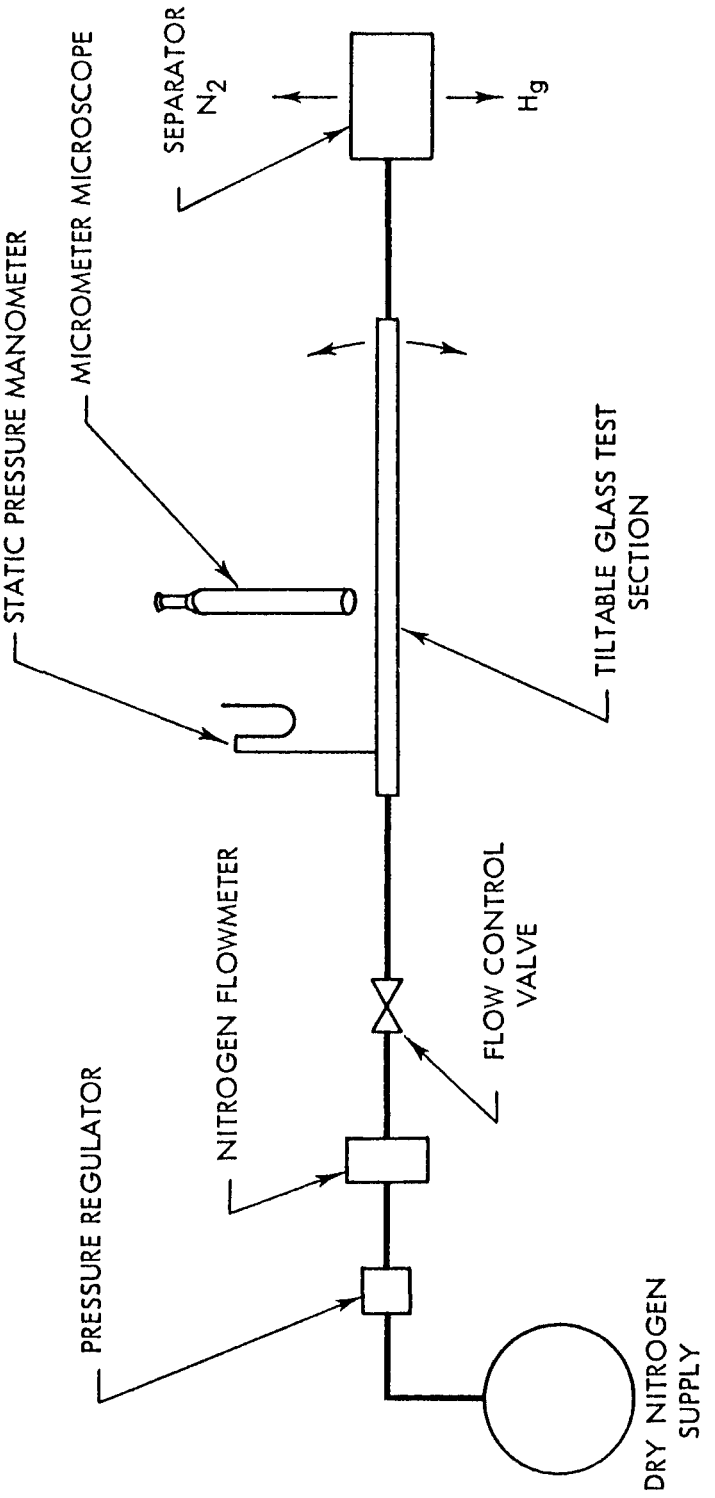

FIGURE 10

Equation 2 now becomes,

$$f\left(\frac{D\rho_g U_g}{\mu_g} \quad ; \quad d/D \; ; \quad \frac{\rho_g U_g^2}{\gamma d}\right) = 0$$

where $\frac{D\rho_g U_g}{U_g}$ is the Reynolds number

and $\frac{\rho_g U_g^2}{\gamma d}$ is the Froude number

For a given tube inclination the Froude number was found to be a function of the gas Reynolds number; therefore the data can be presented as d/D versus the gas Reynolds number for a given tube inclination. The purpose of the tests is to determine the gas Reynolds number at which d/D is independent of gravity, that is, tube inclination. When the term, $\rho_g U_g^2/\gamma d$, is low in magnitude it can be expected that the droplet size ratio is influenced by gravity.

Figure 11 shows a plot of the data obtained from the nitrogen-mercury test rig of Figure 10. The ratio d/D is plotted versus the gas Reynolds number for tubes of different size tilted both upwards and downwards. A measurement of a critical mercury droplet size obtained in a mercury condenser in zero gravity is also shown. The source of this droplet measurement in zero gravity is discussed in the section entitled "Zero-Gravity Tests". Also plotted in Figure 11 is the ratio of laminar boundary layer thickness versus the gas Reynold's number in order to afford a comparison between the droplet size and the thickness of the laminar sublayer. The equation used for computing the thickness of the laminar sublayer is, $\delta/D = \frac{25}{(Re_g)^{7/8}}$

which can be found in any standard text on boundary layer fluid mechanics. Note in Figure 11 that as the critical Reynold's number is reached (4000 to 2000), the laminar boundary layer fills the tube and δ/D equals R/D equals 0.5. The scatter in droplet size measurements is caused by gravity since some of the droplets were measured while clinging to the side of the tube and some were on the bottom. Apparently the force of gravity played some

DROP DIAMETER VS CRITICAL GAS REYNOLDS NUMBER FOR ENTRAINMENT

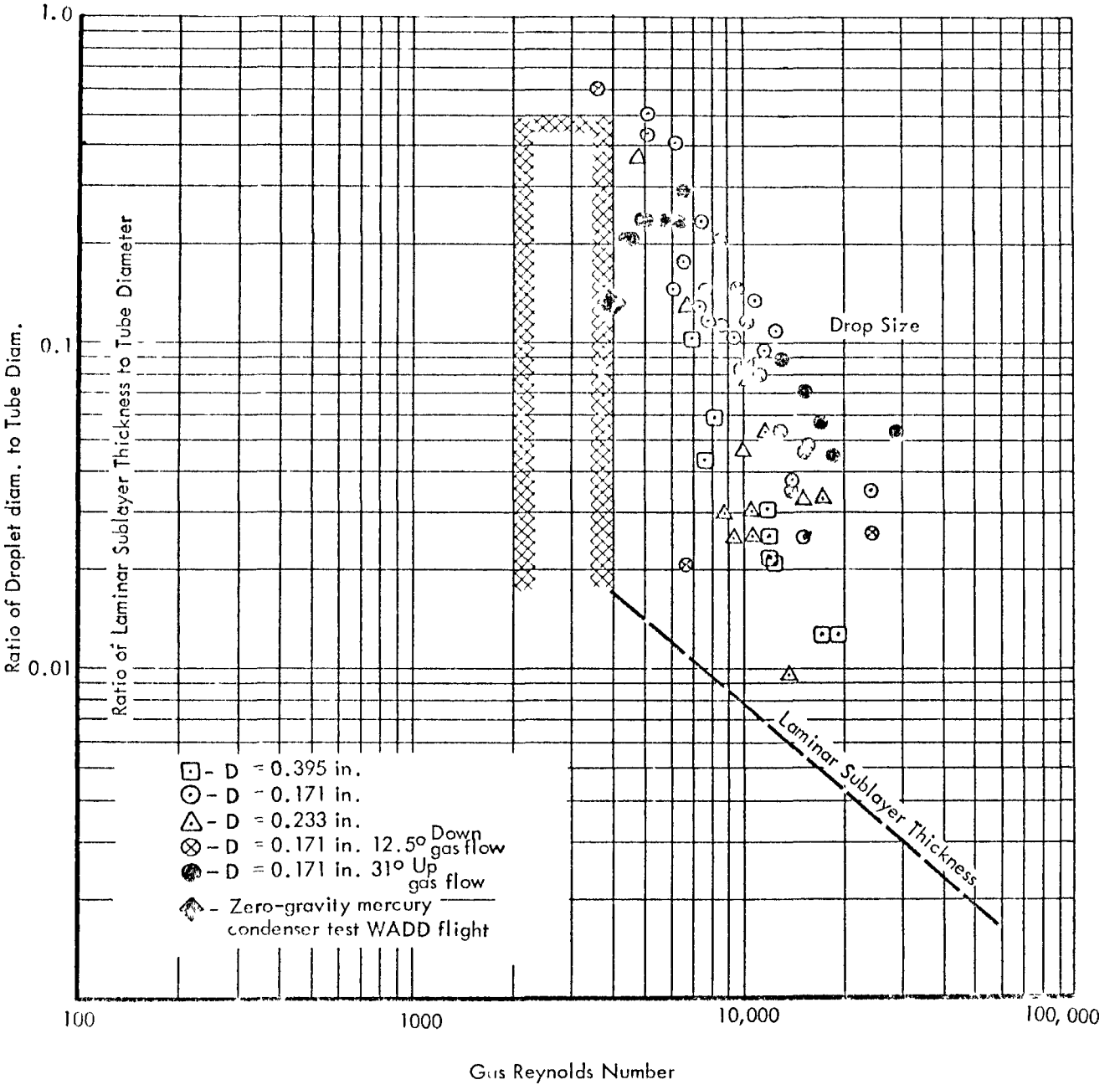

FIGURE 11

role in the incipient motion of the droplet. In addition the tube was oriented in three positions with respect to the gas flow direction, namely, tilted upward, horizontal and tilted downward. In Figure 11 note that the droplet measurements are greater than the laminar sublayer by several factors and that the size of a liquid mercury droplet in mercury vapor in zero gravity (diamond-shaped symbol) appears to be less than the size of liquid mercury droplets in nitrogen gas in a one-gravity environment. This means that data obtained in an earthbound nitrogen-mercury rig are conservative since droplets are smaller in zero gravity and that the flow regime is less likely to be affected by gravity disturbances. Support to this statement is given in Figure 12 in which the ratio of the gas pressure acting on the droplet to weight force of droplet (Froude Number) is plotted versus the gas Reynold's Number. For Reynold's numbers less than 8000, the ratio of inertia to gravity force is of the same order of magnitude, indicating that a condenser designed for Reynold's number lower than 7000 may show changes in performance (changes in inventory and pressure drop) when taken from a one-gravity environment into a zero-gravity environment. Note Froude numbers in the range 100 to 1000 for Reynold numbers greater than 15,000. As mentioned before, indications are that the actual Reynold's numbers for mercury condensing are somewhat lower for a given Froude number.

The effect of gravity in critical droplet size is further illustrated in Figure 13 in which the ratio of gravity to inertia force (reciprocal Froude number) is plotted versus the gas Reynold's number for the case of upward and downward flow of gas. As expected for low Reynold's numbers, droplets are smaller for downward flow than for upward flow since gravity and gas pressure both act in the same direction and therefore both aid in droplet entrainment. As the ratio of gravity to inertia force approaches zero at high Reynold's numbers, the two curves merge, indicating that the role played by gravity becomes negligible. At a Reynold's number near 20,000 the effect of gravity seems to disappear, and according to Figure 12, at a Reynold's number of 20,000 the ratio of inertia to gravity is about 300.

The reason for relating critical droplet size to gas Reynold's number in Figures 11, 12, and 13 is that a relationship is believed to exist between the laminar sublayer thickness - which is also a function of gas Reynold's number - and the critical droplet diameter.

The phenomenon of gas entrainment of mercury droplets is closely related to the subject of sediment transportation which is usually

Froude Number of Mercury Droplets versus Gas Reynolds Number of Pipe

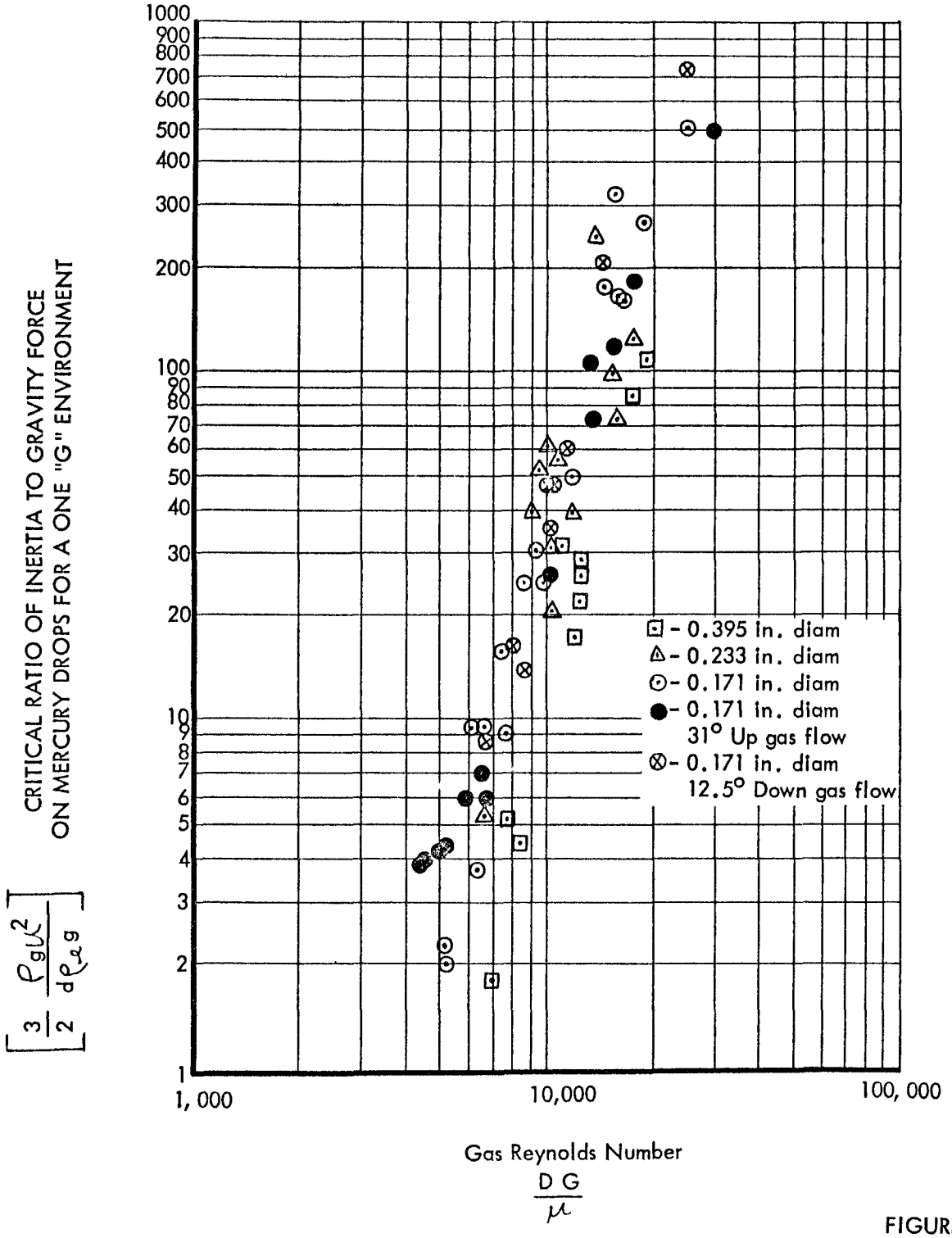

FIGURE 12

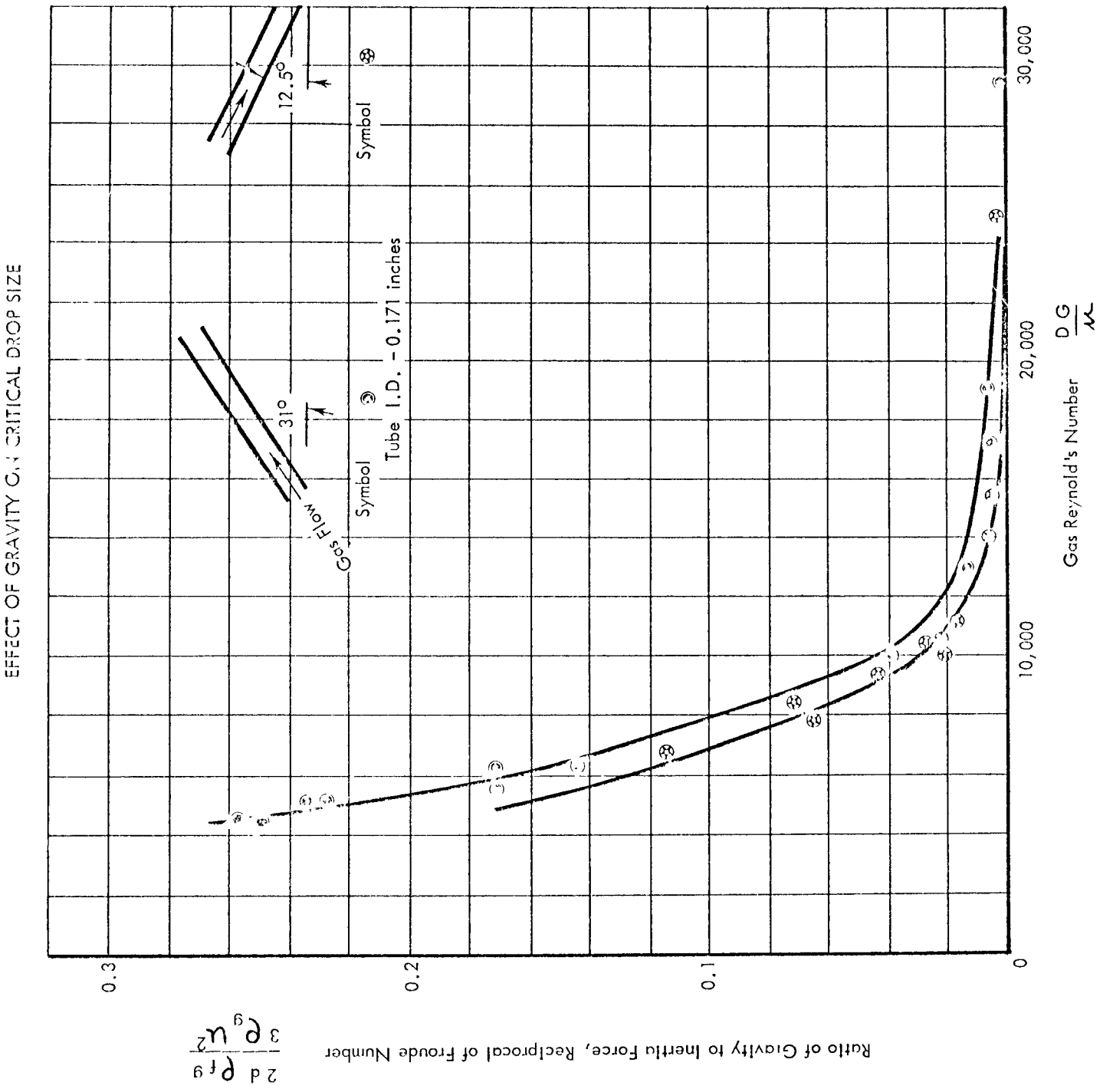
EFFECT OF GRAVITY ON CRITICAL DROP SIZE
Gas Flow
12.5°
31°
Symbol
Tube I.D. - 0.171 inches
Symbol
0.3
0.2
0.1
0
10,000
20,000
30,000
Gas Reynold's Number $\frac{DG}{\mu}$
Ratio of Gravity to Inertia Force, Reciprocal of Froude Number $\frac{2d\rho_{fg}}{3\rho_g u^2}$

FIGURE 13

covered in texts on hydraulics.* Here the transportation rate of sediment is related to the tractive force of the stream. The tractive force required to cause incipient movement of sediment is referred to as the critical tractive force and is closely analogous to the vapor flow rate and the maximum drop sizes to which the condensate can grow before movement begins in a condenser. Various investigators in the fluid of sediment transportation have noted an exponential relationship between particle diameter and the critical tractive force. They noted a change in slope of the function when a certain particle diameter was attained. This was attributed to a change in boundary motion regime depending upon the magnitude of submergence of the surface particle within the laminar boundary layer. Apparently the ratio of particle diameter to laminar boundary layer thickness becomes the essential parameter. This ratio has the same significance as the ratio of the size of the surface roughness projections to the laminar boundary layer thickness in the case of pipe roughness and friction factors. Many investigators in the field of sediment transportation feel that the ratio of particle diameter to the boundary layer thickness plays an essential role in determining not only the beginning of movement but the form of the function at incipient motion.

Zero-Gravity Tests

These tests were conducted with TRW test apparatus aboard the C-131-B aircraft at WADD. The tests were part of the SNAP II - sponsored OFFBACE program investigating the fluid mechanics aspects of a Rankine cycle power plant in a zero-gravity environment. WADD flew the airplane through trajectories which produced conditions of weightlessness (zero "G"), 2.55 "G" and unity "G".

Figure 14 presents photographs of mercury condensing during different magnitudes of body forces acting normal to the tube axis. The photographs were produced from high speed motion picture films taken at 500 frames per second (thirty times normal speed).

These photographs show mercury droplets produced in a 0.136 inch inside diameter tube approximately 12 inches long with inlet vapor Reynold's numbers in the range of 2000 to 4000. Droplet measurements taken from the high speed films and presented in Figure 15 show a change in drop size distribution when going from zero "G" to

* Fluid Mechanics for Hydraulic Engineers by Hunter Rouse, New York: McGraw-Hill Book Co., 1938.

MERCURY CONDENSING IN A 0.136 INCH ID TUBE 12 INCH EFFECTIVE CONDENSER LENGTH FLOW FROM LEFT TO RIGHT

Photographs From TRW Apparatus Aboard C-131-B Aircraft Flying Zero-Gravity Maneuvers at WADD, March 18, 1960

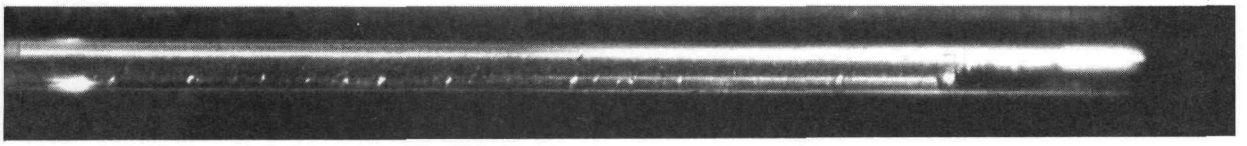

INLET REYNOLDS NUMBER = 1950
2.55 "G"

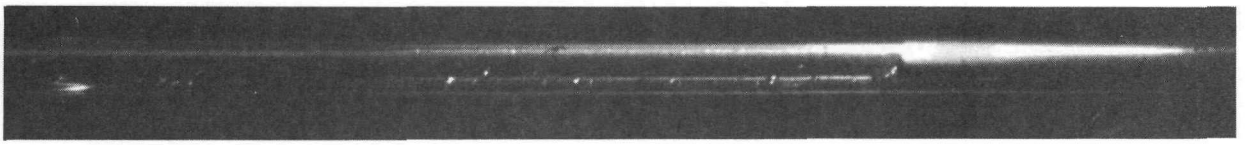

INLET REYNOLDS NUMBER = 3440
1.0 "G"

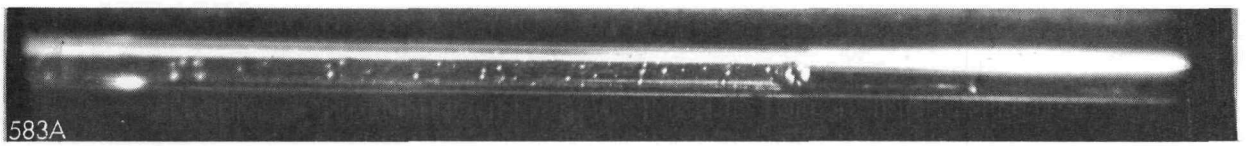

INLET REYNOLDS NUMBER = 3860
0 "G"

FIGURE 14

SPREAD IN DROPLET SIZE OF VISIBLE MOVING DROPLETS
IN MID-SECTION OF CONDENSER TUBE WITH ACCELERATION

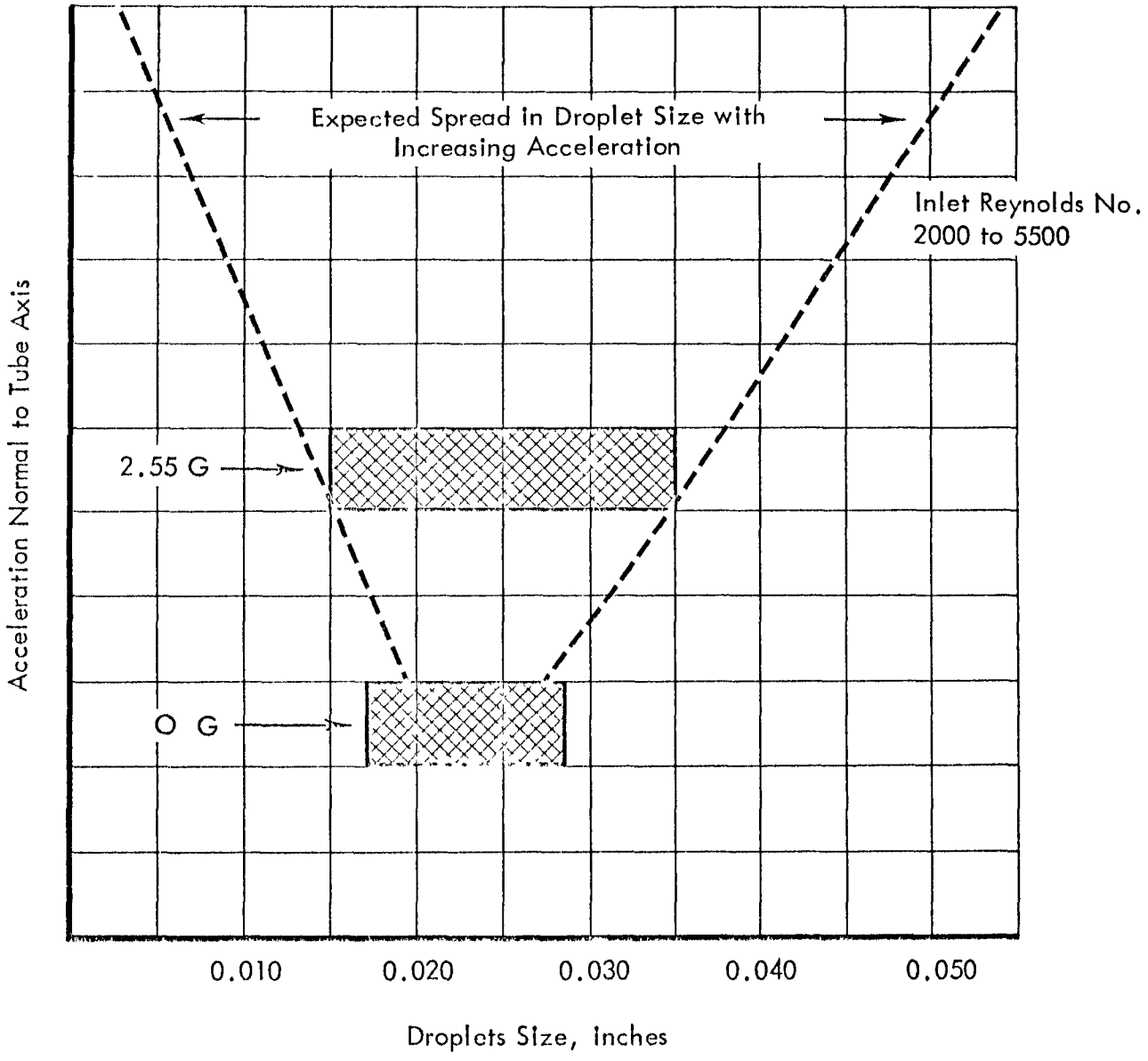

FIGURE 15

2.55 "G". This means that the flow regime is sensitive to body force disturbances and that changes in mercury inventory and pressure drop would occur as a result. This sensitivity is attributed to the low vapor Reynold's number and the resulting low Froude number of the droplets. A high Reynold's number condenser would be insensitive to body force disturbances except in the region near the interface where the local vapor velocity and gas Reynold's number approach zero.

Growth of droplet size due to agglomeration near the liquid interface further increases the sensitivity of the flow pattern to gravity disturbances. Tapering the tube is a means of remedying the situation since vapor velocities are maintained high along the tube. Drop agglomeration which depends on the volumetric flow ratio of liquid to vapor becomes a problem when the mixture quality becomes low for both straight and tapered tubes. The agglomeration effect is brought out by Equation 2 which has the critical droplet size as a function of the droplet concentration ratio of moving drops to stationary growing droplets on the wall.

The spread in drop size due to gravity shown in Figure 15 is caused by gravity's inducing incipient drop motion in the upper part of the tube and by gravity's retarding movement in the lower portions. Therefore, droplets entrained in the upper region of the tube will become smaller while droplets in the lower region will get larger. The reason for some spread in drop size even at zero gravity is the fact that the data were evaluated near the mid-section of the tube where small droplets born near the condenser inlet in a relatively high vapor Reynold's number are mixed with larger droplets originating further downstream where the local vapor Reynold's number is relatively low.

Figure 16 shows droplet size measurements taken near the condenser inlet where the spread in droplet size should be at a minimum. The data are plotted as a cumulative curve. Since the measurements were made in zero gravity and near the condenser inlet, the curve should have a steep slope. Ideally the curve would be vertical if only drops of one size were present. The curvature toward the right of the median indicates some large drops are present due to possible liquid "carry-over" from the boiler or agglomeration or condensing in the elbow or fitting upstream of the tube. The curvature toward the left near the bottom section of the curve is so drawn as to indicate some possibility of entraining droplets of sizes smaller than the minimum size measured. The value for the median drop size is plotted in Figure 11 for comparison with drop

CUMULATIVE CURVE OF DROPLET DISTRIBUTION
IN ZERO-GRAVITY MERCURY CONDENSER

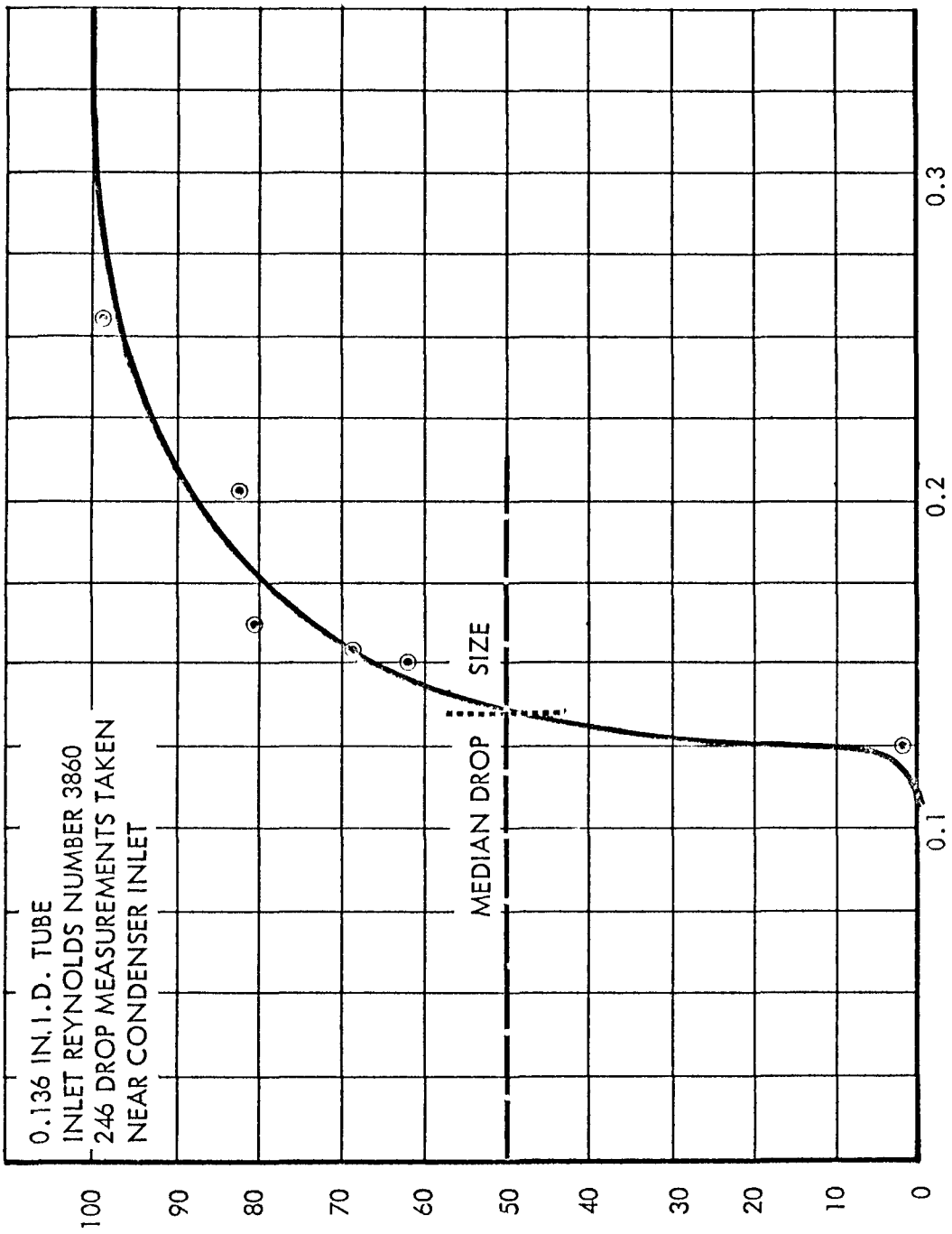

FIGURE 16

size data obtained in nitrogen gas. The low position of this test point with respect to all the others indicates that conditions in zero gravity and in mercury vapor should be more favorable for flow regime stability than indicated by earthbound tests using nitrogen gas.

3.3 Condenser Pressure Drop

Pressure drop in mercury condensers was measured on both straight and tapered tubes. These tubes were operated in both the horizontal position and inclined upwards from the horizontal. Condensing temperatures ranged from 500°F to 640°F. The total range of Reynolds numbers, measured at the condenser inlet, was from 12 to 12,000.

The ratio of condenser length to condenser inlet diameter (L/D), ranged from 24 to 460. The data were correlated over this range and found to agree with adiabatic two-phase flow data at high Reynolds numbers.

3.3.1 Pressure Drop Apparatus

In all cases the apparatus was fabricated from Pyrex glass. The condenser tube was joined to a glass bulb boiler containing a pressure tap. Glass was used for ease of fabrication and to secure a leak proof apparatus. The greatest advantage of using glassware was that the condensing process could be visually observed and pressure and flow rate could be measured directly in the apparatus.

Figure 17 is a schematic of a typical test setup. The boiler was partially filled with liquid mercury and submerged in the liquid lead bath. The vacuum pump was turned on and the condenser tube was opened to the degassing line. The air was drawn off and the mercury vapor flowed into the cold condenser tube and condensed. The valve between the vacuum pump and the boiler pressure manometer was opened for an instant to draw vapor into the tube. This vapor condensed and formed a liquid plug between the "U" tube manometer and boiler (the boiler pressure manometer has an inside diameter of 0.10 inch and therefore will hold a stable liquid plug). With the end of the condenser tube closed off, the flow rate was measured by timing the increase in length of the condensate in the condenser tube. The pressure at the liquid-vapor interface in the condenser was measured by liquid height between the condenser tube and the liquid surface in the condensate sump. Both boiler and condenser pressures were referenced to the atmospheric pressure.

In most cases natural convection on the outside of the tube was found to cool the condenser adequately. At the high Reynolds numbers a fan was

TYPICAL MERCURY CONDENSER TEST SET-UP

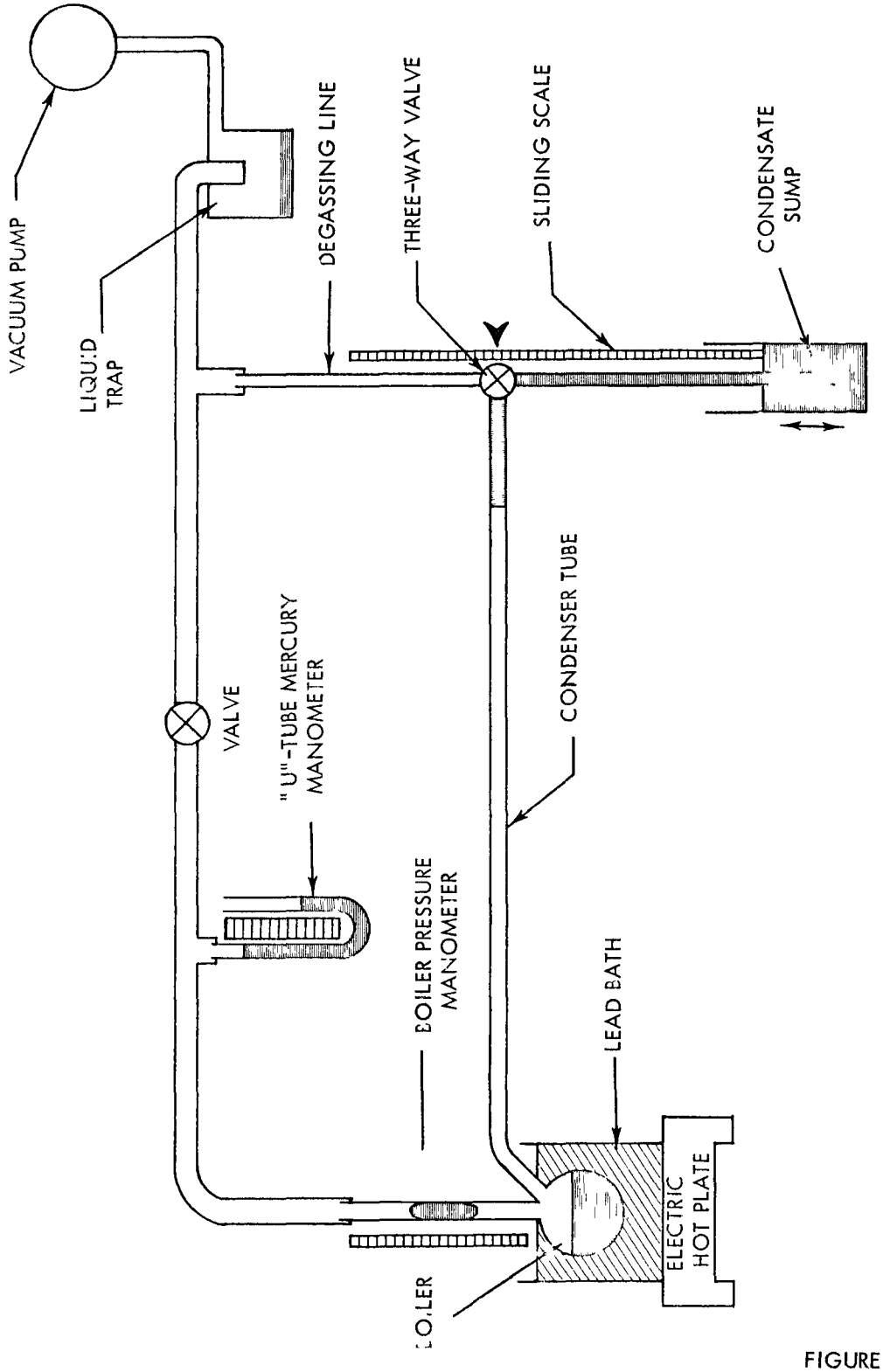

FIGURE 17

used to blow air over the tube to achieve higher cooling rates. The flow rate in the tube could be varied by changing the effective condenser length by controlling the condensate liquid length in the condenser tube.

Three separate condenser tubes were tested. The tapered condenser tube was 39 inches long. This tube was tapered by drawing it out by hand. Consequently the actual taper could not be predetermined. Figure 18 shows the measured inside diameter of this tube along its length. This tube was operated both horizontally and inclined at 43 degrees upwards from the horizontal.

A straight tube 0.157 inch inside diameter and four feet long was operated inclined at 15 degrees with the horizontal. To obtain higher flow rates in the tube, a six foot long tube of 0.150 inch inside diameter was tested.

The range of flow rates obtained in each tube was directly proportional to the tube length. To obtain higher flow rates, and consequently higher Reynolds numbers, tubes longer than six feet must be used.

A table of all the pressure drop data is obtained in Appendix II. An examination of this data reveals both reproducibility and consistency.

3.3.2 Condenser Pressure Drop Test Results

A convenient way to present two-phase flow pressure drop data is as a ratio between the actual pressure drop to that which would occur if one phase were flowing separately. This ratio is defined as Φ.

The minimum value of Φ is unity since the addition of a second phase into a duct having a flow of fluid cannot decrease the pressure drop to a value less than that occurring for the original flow.

For condensing, Φ is defined as the ratio of the pressure drop for condensing a vapor of unity quality, excluding momentum pressure recovery, to the computed pressure drop which would occur for the vapor alone flowing without liquid present. Thus,

$$\Phi = \frac{\Delta P_{TP}}{\int_{x=1}^{x=o} f \frac{(GX)^2}{\rho_v 2g_s} \frac{dL}{D}} \qquad (3)$$

G = total mass velocity
ρ_v = vapor density
X = quality
f = friction factor
L = length
D = diameter
ΔP_{TP} = two-phase pressure drop

where ΔP_{TP} represents the frictional two-phase pressure drop corrected for momentum effects.

The differential length, dL, can be replaced by a differential quality change dX if the condensing load is defined along the tube length. In vapor condensers, friction factor and diameter can all vary along the tube. The Φ defined by Equation 3 is an integrated mean value as obtained by a condenser which in effect is an integrating device giving integrated measurements.

The pressure drop for vapor alone is computed as though the reduction in vapor fraction along the tube were accomplished by extraction of the vapor rather than by condensation. As mentioned in the previous section, the upstream pressure is measured at the boiler and the downstream pressure is measured after the liquid-vapor interface. Therefore the measured pressure drop must be corrected for the acceleration at the condenser inlet and the momentum pressure recovery must be accounted for so that the pressure drop represents only the drag forces due to the liquid droplets and the wall shear stress on the flowing liquid-vapor mixture. These corrections are given in Appendix I.

In computing the pressure drop for vapor flowing alone, the changing mass flow rate of vapor, the vapor density and the friction factor along the tube are taken into account. In the case of a tapered tube the variable diameter along the tube should be included. The calculation procedure for the gas only pressure drop is given in the appendix.

By dimensional analysis it can be shown that for two-phase flow:

$$\underline{\Phi} = f\,(Re,\ Fr,\ \rho_g/\rho_\ell\ ,\ \mu g/\mu_\ell)$$

For liquid mercury the properties may be considered as constants over the range of temperatures for which pressure drop data were obtained. This includes the design point for the SNAP II condenser.

Therefore the liquid properties do not enter the correlation. For condenser pressure drop data it was found that $\underline{\Phi}$ could be expressed as:

$$\underline{\Phi} = f\left[Re_o\left(\frac{\bar{v}_g}{10}\right)^{1.25}\right]$$

where Re_o is the inlet vapor Reynolds number
$\bar{v}_g$ is the mean vapor specific volume evaluated at average condenser pressure, ft^3/lb

MEASURED TAPERED TUBE INSIDE DIAMETER

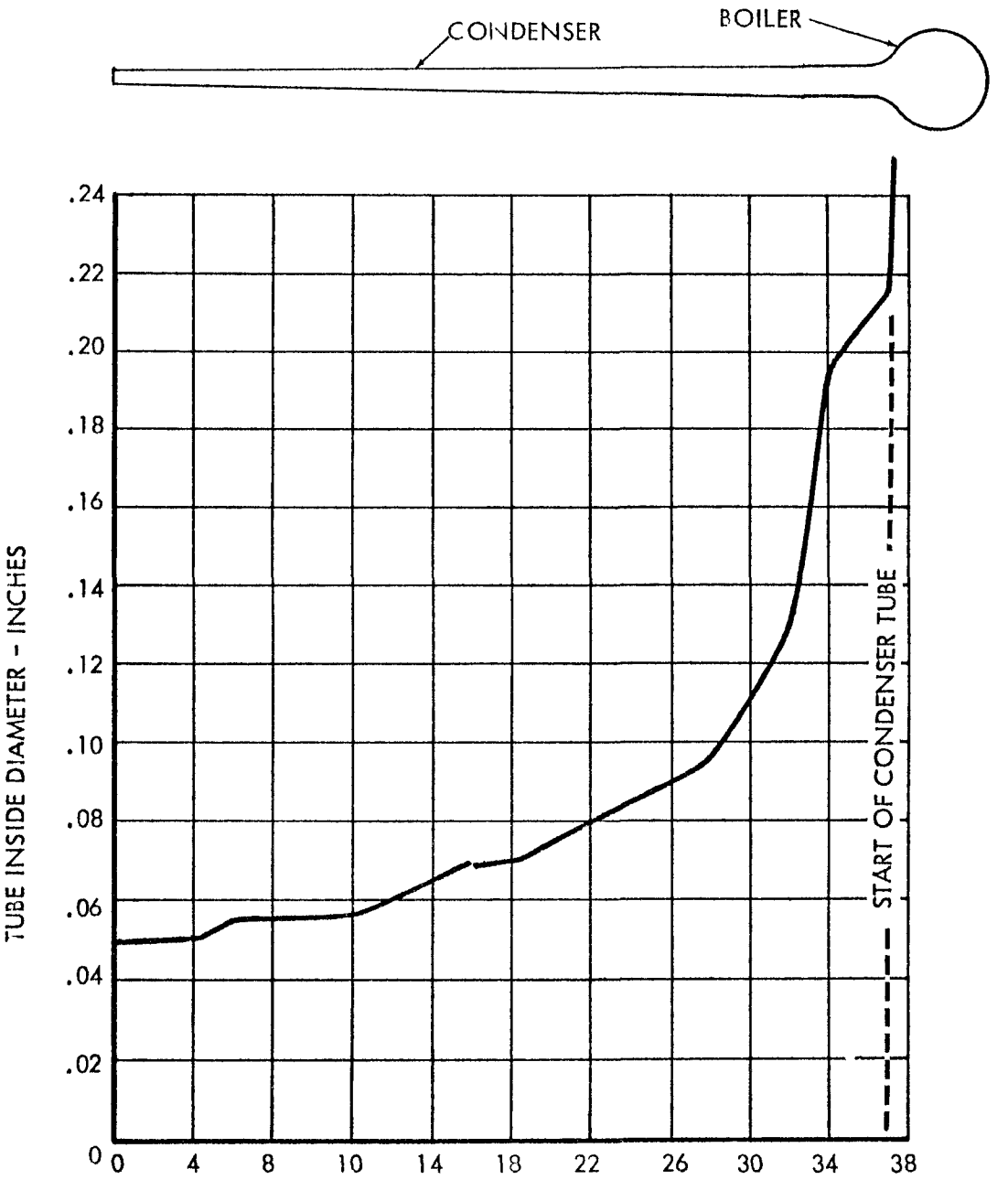

FIGURE 18

The Froude number was found to be a function of the Reynolds number, as shown in Section 3.2.1.3. The effect of Froude number was investigated by changing the attitude of the condenser tube.

To present the results, the specific volume is normalized by dividing by 10 which is near the average value for all of the test data. The mean specific volume, as shown in Appendix I, is the specific volume at the average of the inlet and outlet condenser pressures. The value of the mean specific volume ranged from 5 to 35 ft^3/lb in these tests.

Figure 19 shows the resulting plot of Φ versus the Reynolds number -- specific volume parameter. Also shown on this plot is the Martinelli correlation for viscous - turbulent flow, * for an average quality of 50 percent and properties evaluated at 600°F. It is remarkable first of all that the parameter $Re_o\ (\bar{v}_g/10)^{1.25}$ which was found to fit the condenser data should also be factorable in the Martinelli parameter, and secondly that the curves through the inclined condenser test data, horizontal condenser test data and the Martinelli correlation should all come together at the same point.

The large value of Φ at the low Reynolds numbers is caused by the presence of large liquid drops. As shown in Section 3.1.2.3, drop size increases rapidly with decreasing Reynolds numbers. The large drops result in a large liquid inventory which raises the pressure drop. At high Reynolds numbers the drop size is smaller than at low Reynolds numbers and the effects of the drops on the pressure drop are less important when compared to the shear stresses on the vapor, as indicated by Φ approaching a value of unity. Also evident in Figure 19 is that values of Φ are higher for the inclined tubes than for the horizontal tubes at the lower Reynolds numbers. This is due again to the fact that at low Reynolds numbers gravity forces become important due to the relatively large drops. The drops are larger in the inclined tubes than in the horizontal tubes due to gravity force opposing the drop movement in the condenser.

It is significant that the highest Φ values were recorded for an inclined tapered tube run at very low values of the parameter $Re\ (v_g/10)^{1.25}$. Data for condensation in a constant diameter tube may not follow the same curve. Furthermore, the variations in performance with orientation may be different for the constant diameter and tapered tubes in the low Reynolds number range due to varying degrees of gravity sensitivity with tube geometry. In a complete formulation of the condensing process, gravity effects and tube geometry effects (e.g. l/D, tube taper, and swirl devices) would be included in the correlating parameters.

*Lockhart and Martinelli, "Proposed Correlation of Data for Isothermal Two-Phase, Two-Component Flow in Pipes", Chem. Eng. Prog., Vol. 45 (39), 1949.

The merging of the curves at a value of 10,000 for $Re_o (\bar{v}_g/10)^{1.25}$ indicates that at this point pressure drop is no longer greatly influenced by the gravity force. The Reynolds number is the same order of magnitude as the parameter $Re_o(\bar{v}_g/10)^{1.25}$. As shown in Section 3.2.1.3, gravity influences become small at Reynolds numbers near 10,000. Therefore all indications are that at Reynolds numbers appreciably lower than 10,000 gravity force variation between one and zero gravity will have an effect on the pressure drop.

As the drops become very small at the high Reynolds numbers Φ appears to be approaching a constant value. When the drops become so small that the liquid-vapor mixture can be treated as an homogeneous fluid, the flow regime is defined as fog flow. In fog flow the liquid and vapor have the same velocity and the specific volume is that of the mixture. The value of Φ for fog flow in a straight tube is 1.5.

The spread in the data of Figure 19 is not excessive compared to other two-phase flow data. Martinelli's data have a spread of ±30 percent and data of other investigators compared to the Martinelli curve show even larger spread as shown in the next section.

Since the value of the pressure drop in the condenser is obtained by taking the differences in manometer readings some inaccuracies are obtained by this method, especially at low flow rates where the pressure drop is a small value. It is expected that some of the data spread is due to these compounded measuring inaccuracies. For Reynolds numbers greater than 1000 the accuracy of Φ is expected to be ± 20 percent due to the apparatus itself. At Reynolds numbers lower than 1000 the spread may be as large as ±100 percent. The additional spread in data above these values evident in Figure 19 is due to the necessarily simplified correlating parameters that do not account for all characteristics of this complex fluid flow field.

3.3.3 Comparison of Condenser Pressure Drop Results to Other Data

Any correlation for particular data can be evaluated by comparing results to published data. As shown in Figure 19, condenser pressure drop data agree with the Martinelli curve at high Reynolds numbers. Figure 20 compares the curves in Figure 19 to three other sets of mercury data obtained at TRW: boiler test data, and mercury-nitrogen two-phase flow data for bare tubes and for tubes with internal springs.

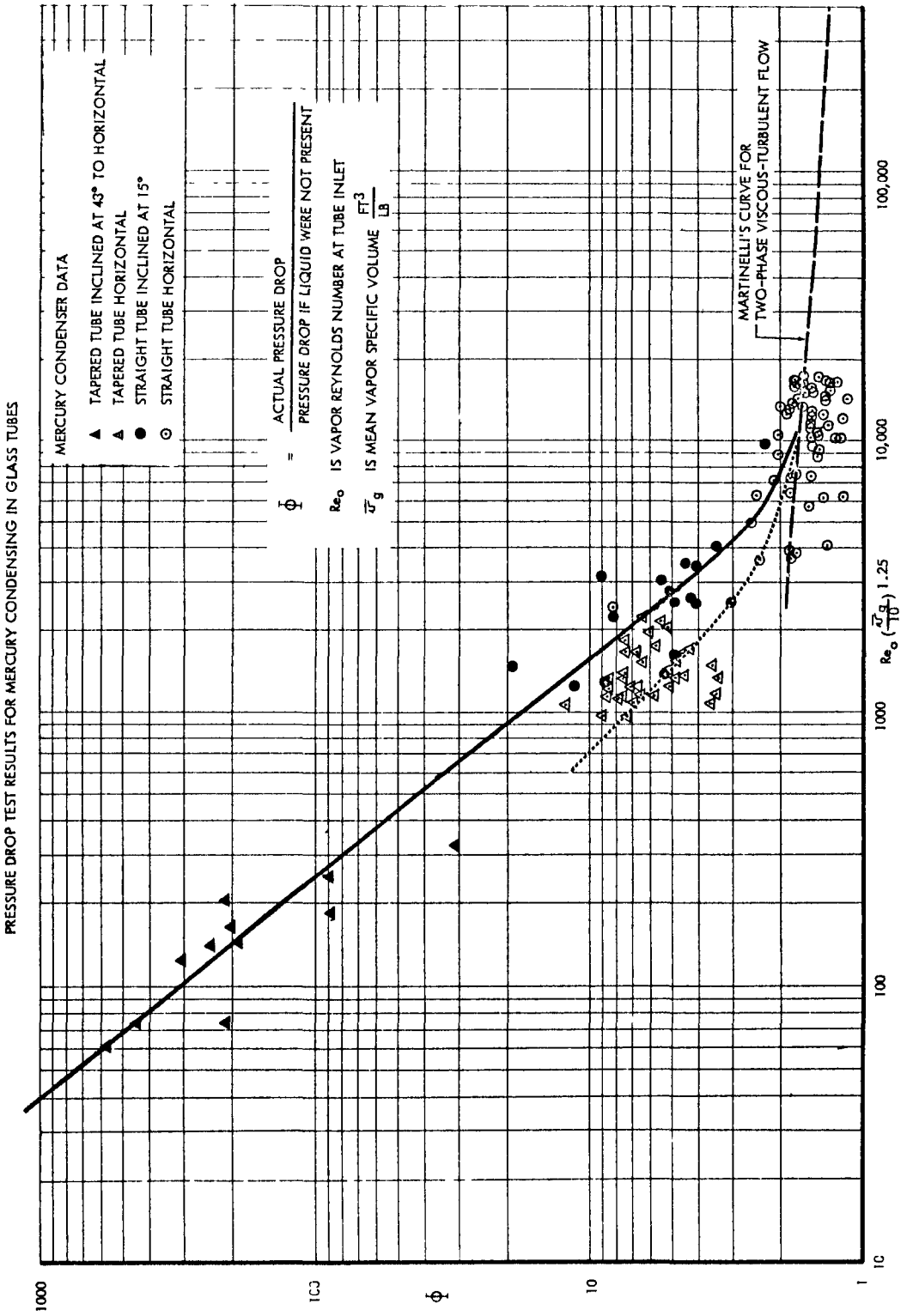
PRESSURE DROP TEST RESULTS FOR MERCURY CONDENSING IN GLASS TUBES
MERCURY CONDENSER DATA
TAPERED TUBE INCLINED AT 43° TO HORIZONTAL
TAPERED TUBE HORIZONTAL
STRAIGHT TUBE INCLINED AT 15°
STRAIGHT TUBE HORIZONTAL
Φ = ACTUAL PRESSURE DROP / PRESSURE DROP IF LIQUID WERE NOT PRESENT
Re_o IS VAPOR REYNOLDS NUMBER AT TUBE INLET
σ_g IS MEAN VAPOR SPECIFIC VOLUME FT³/LB
MARTINELLI'S CURVE FOR TWO-PHASE VISCOUS-TURBULENT FLOW
Φ
Re_o (σ_g/σ_f) 1.25
1000
100
10
1
1C
100
1000
10,000
100,000

FIGURE 19

COMPARISON OF MERCURY PRESSURE DROP DATA

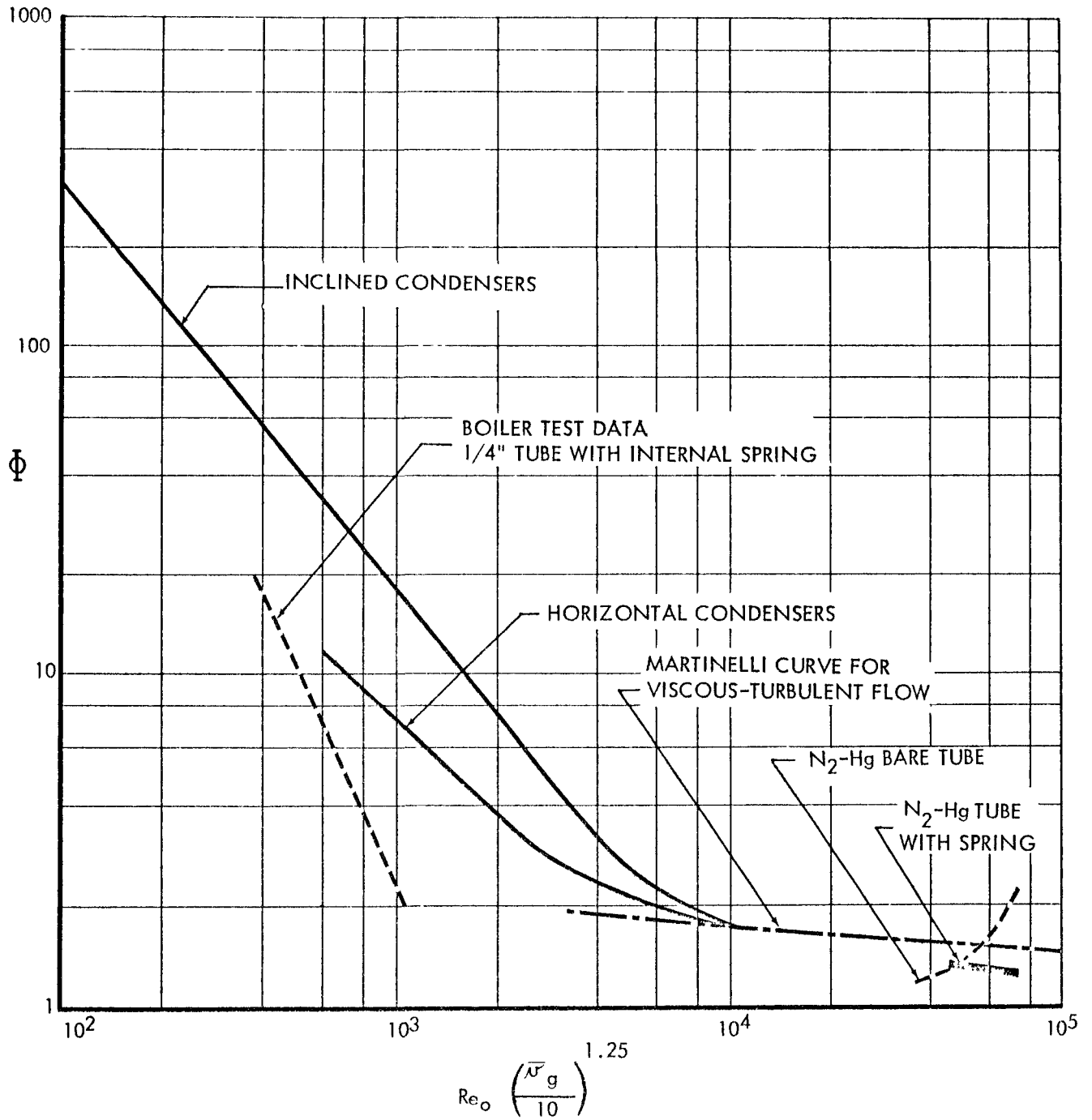

FIGURE 20

Data for boiling mercury at near 100 psi in 1/4 inch tubes with internal springs show the same trends with Reynolds number as the condenser data. In this case the Reynolds number represents the outlet value and the actual Reynolds numbers are between 10^4 and 10^5. The value of Φ for the boiler data is not expected to agree with condenser data because flow patterns vary. The internal springs in the boiler keep drops swirled to the walls whereas drops may flow uniformly over the entire cross section of the tube in the condenser.

Mercury-nitrogen two-phase flow data obtained in a bare tube passes through the Matinelli curve. This deviation from the Martinelli curve agrees with two-phase flow results of other experimenters and can be attributed to gravity effects (relatively low Froude number).

Figure 21, reproduced from WADC Technical Report 55-422*, is an example of the poor comparison of experimenters' data with some proposed correlation such as Martinelli's. As explained in the report, "This figure (Figure 21) indicates clearly that the correlation proposed by Martinelli does not predict the data as completely as one would like. In addition, these data confirm the objections of Jenkins, i.e., that a definite trend with liquid rate exists which is not accounted for in the correlation. The correlation is seen to be partially successful in predicting the data at high air rates (low value of abscissa). At low air-water ratios the data deviate to such an extent that the correlation is considered useless even though the two assumptions on which the correlation was based are fulfilled." In Figure 21 agreement with Martinelli's correlating curve is reached at the higher flow rates where the Froude number becomes relatively large.

The effect of gravity was also noted in mercury condensation tests at TRW. In the low Reynolds number range where the droplet Froude number is low, the inclined tube indicated higher pressure drops than the horizontal tube. At the higher Reynolds numbers (above 10,000), the differences between the inclined and horizontal tube disappeared because inertia is large compared to gravity.

Mercury-nitrogen test data at TRW for the bare tube without swirl inserts show increasing values of Φ with Reynolds number, resembling the curve

---

* Gresham, W.A., P.A. Foster, R.J. Kyle. "Review of the Literature on Two-Phase (Gas-Liquid) Fluid Flow in Pipes," Part I, WADC Technical Report 55-422, Georgia Institute of Technology, June 1955.

EXPERIMENTAL DATA OF DUKLER FROM "REVIEW OF THE LITERATURE ON TWO-PHASE FLUID FLOW IN PIPES"— WADC TECHNICAL REPORT 55-422

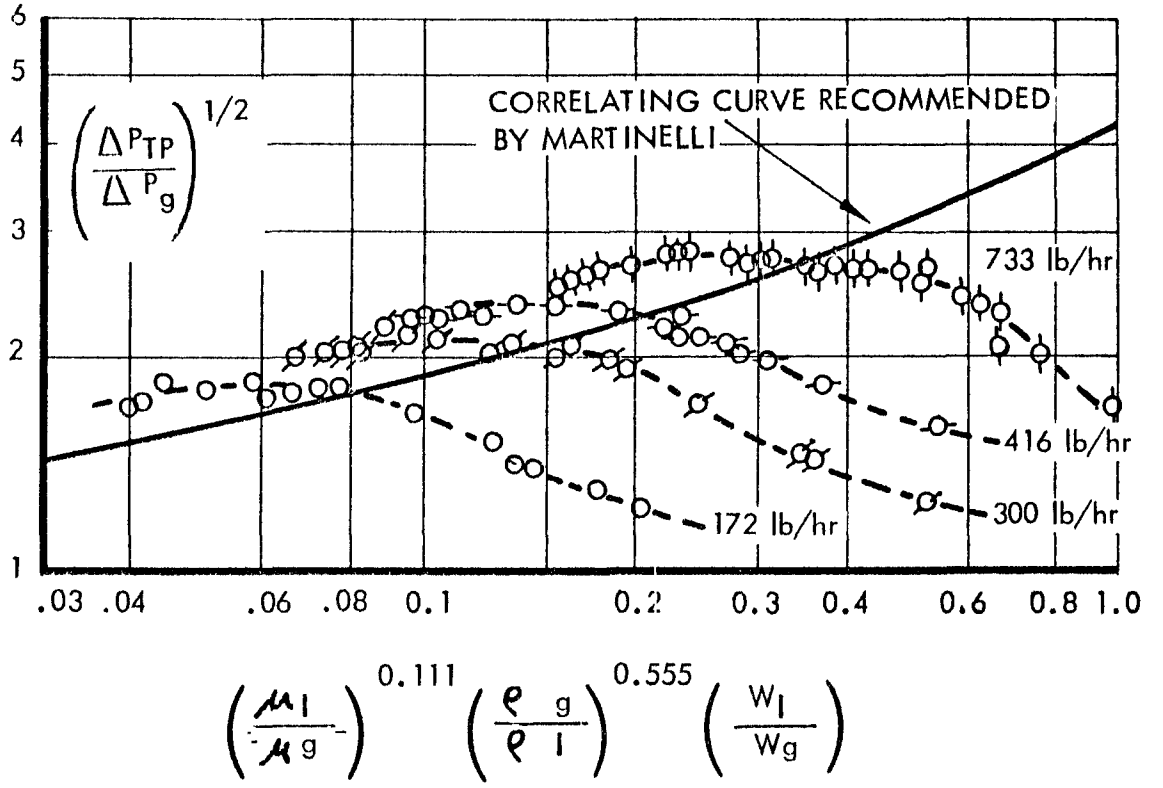

FIGURE 21

of Figure 21. The appearance of flow at low Reynolds number indicated stratification of mercury droplets near the lower portion of the tube. At higher Reynolds numbers the droplets appeared homogeneously dispersed throughout the cross section of the tube.

Rig sensitivity was responsible for the effect of gravity in the mercury-nitrogen rig. Evidently the mercury atomizing nozzle and the mixing length between nozzle and test section produced mercury droplets larger than those produced by the condensation process.

Data obtained in the mercury-nitrogen rig for tubes with spring inserts did not exhibit gravity effects (see Figure 20). Because acceleration forces produced by the spring inserts are radial and are large enough to mask out the 1 "G" due to gravity, Φ remains relatively constant with Reynolds number. An exact correlation can not be expected, since a slightly different flow pattern is produced, i.e., droplets are swirled and forced to the tube wall in a tube with swirl inserts and are randomly distributed in a bare tube.

Local low vapor velocities and droplet Froude number will make any condenser somewhat sensitive to body forces as the quality approaches zero. This sensitivity can be minimized by tube tapering. Visual observation during tests in tapered tubes showed a uniform cloud of mercury droplets moving steadily, without evidence of slugging, toward the interface in both inclined and horizontal tubes.

3.4 The Influence of Non-condensable Gas upon the Condensation Process

It is well known that the presence of a non-condensable gas in a condensing vapor greatly influences the condensing heat transfer coefficients. Heat Transmission by McAdams presents some empirical equations by which the effect of non-condensables on the heat transfer coefficient can be estimated.

When vapor is condensed in tubes by forced convection at high velocities, the presence of a sufficient quantity of gas may mean the formation of gas plugs in the condensation lines. If the volume of gas plugs approaches the volume of the condensate pump, erratic pumping or even flow stoppage may result. Since the condensate pump on the SNAP II system is small in size, care must be taken to prevent a complete power plant failure due to the presence of a gas plug in the condensate line.

Since surface tension and small diameters are required to create a stable liquid-vapor interface between the subcooler and the condenser, gas plug formation is exceptionally favorable. Experimental measurements have clearly indicated the physics of the phenomenon. Figure 22 shows a temperature traverse made along the

EFFECT OF NON-CONDENSABLE GAS ON CONDENSER WALL TEMPERATURE.

T/T_{inlet} RATIO OF ABSOLUTE TEMPERATURES.

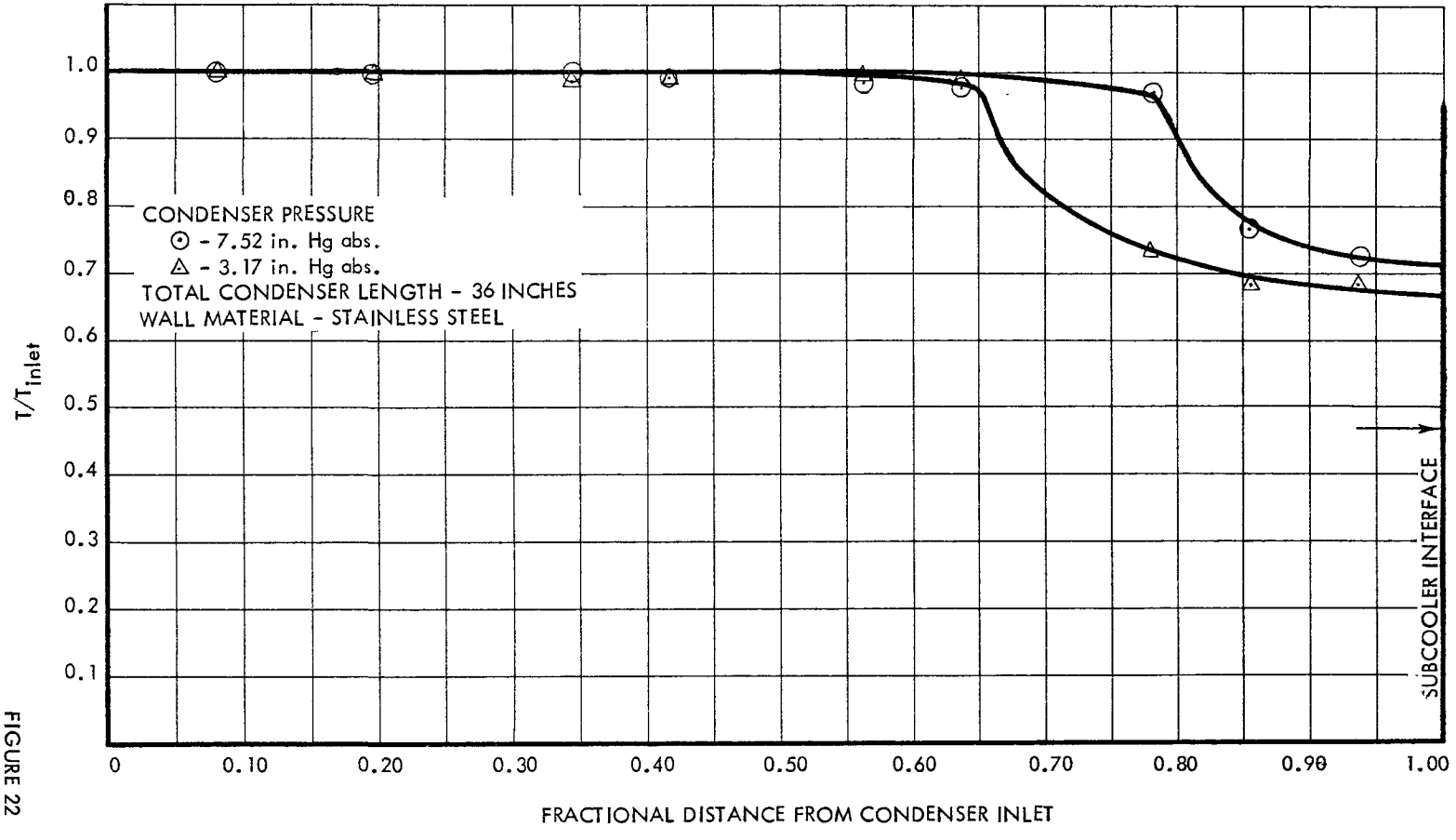

FIGURE 22

wall of a condenser containing condensing mercury vapor and air. The condenser was operated vertically with flow downward. The interface position was determined by a sight glass connected between the condenser inlet and liquid discharge line. The decreasing condensing temperature near the subcooler liquid-vapor interface clearly shows that the gas-to-vapor concentration ratio increases very rapidly as the end of the condenser is approached. The low velocities of the vapor-gas mixture in this region produce an ideal situation for the formation of a gas plug. The flowing condensate droplets are slowed to a half near the interface due to the relatively stagnant region of non-condensables. These droplets then grow by agglomeration until they fill the tube cross section and entrap a volume of gas. A new subcooler liquid interface is thus formed and downstream a gas plug moves toward the condensate pump. Figure 22 shows that for low condenser pressures the region occupied by the gas before the subcooler interface is large, whereas at higher pressure this same region is compressed. During the experiments it was observed that large gas plugs were formed at low condenser pressures and smaller plugs at higher pressures. Also when the gas was removed by means of a vacuum tap just above the interface the temperatures near the interface approached the saturation temperature.

Equations for predicting the form of the temperature profile shown in Figure 22 can be readily set up by applying the convection heat transfer equation, the equation of state for a mixture of saturated vapor and gas, and by assuming that the mixture is always at the dew point and at a constant total pressure.

Methods of gas removal are now under consideration and experiments are being devised. Since there is a high concentration of gas upstream of the subcooler interface and in the plugs, separator type devices are not contemplated since the gas is already in a separated state. The removal of gas in the form of a plug can be accomplished by means of a porous tube wall having pore sizes sufficiently small to prevent the non-wetting mercury from flowing out. (See Figure 23) This phenomenon is presently being used in porous bed boiling experiments.

The porous wall section should be inserted in the coldest part of the subcooler, since here the vapor lost from the non-wetting mercury interface is at a minimum. For example, the vapor pressure above a mercury interface (see Figure 23) at 420°F is 0.54 psia, whereas the pressure of the gas plug will be equal to condenser pressure which is 6 psia. The porous section must be designed to lose not more than a predetermined, permissible amount of mercury over the operating life of the power plant.

GAS REMOVAL BY MEANS OF POROUS WALL

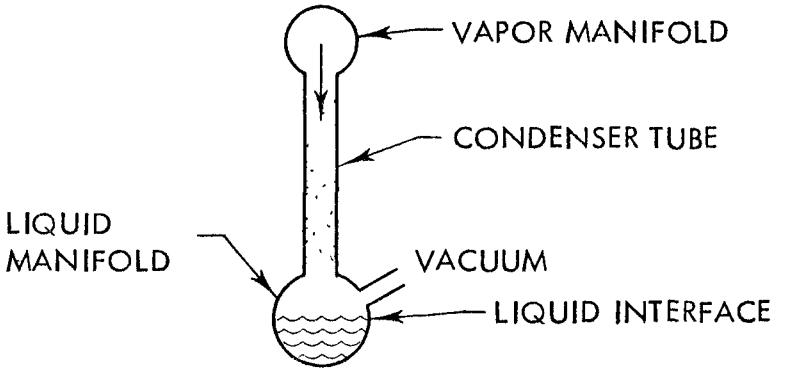

METHOD OF GAS REMOVAL IN PCS TEST RIG

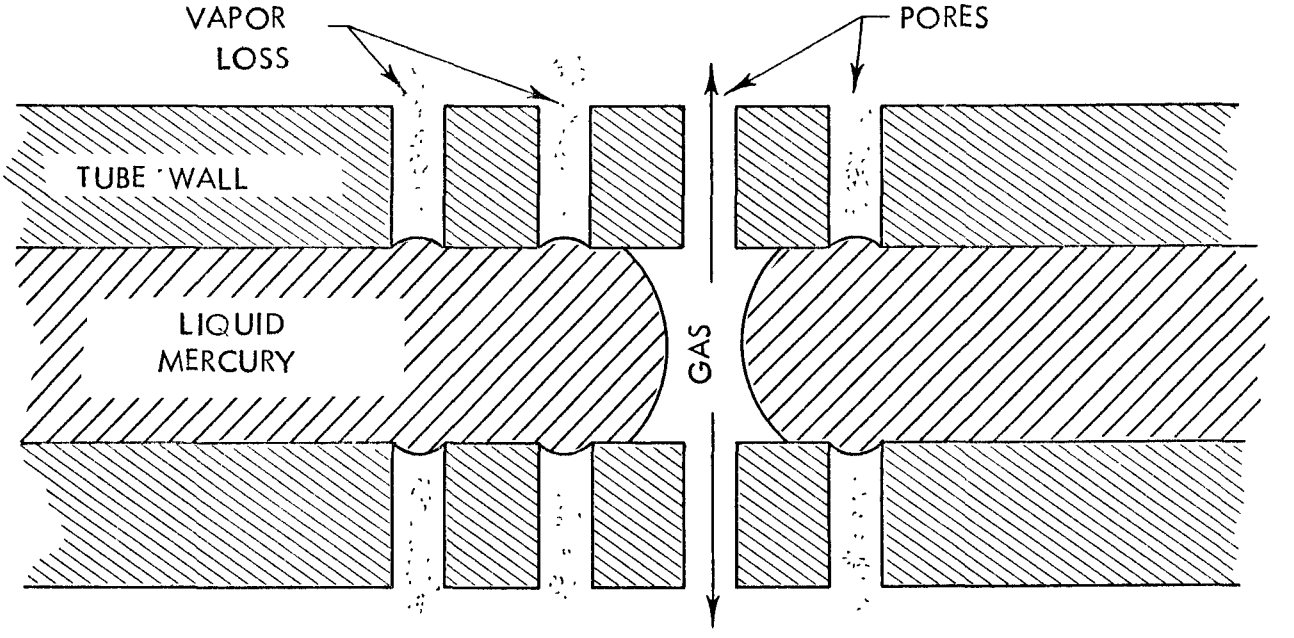

FIGURE 23

4.0 CONCLUSIONS

1. Interfacial stability can be maintained through proper selection of tube diameter.

2. Two-phase flow, mercury-nitrogen pressure drop test data can be used to approximate condenser pressure drop.

3. Condenser inventory is approximately eleven times the weight of vapor only in the condenser tube.

4. Flow regime stability is a function of Reynolds number; increasing Reynolds numbers increase stability. At Reynolds numbers less than 10^4, inventory and pressure drop will change due to changes in magnitude and direction of the body force.

5. At Reynolds numbers greater than 10^4 the condenser pressure drop will be less than twice that if vapor only were flowing in a condenser tube.

6. If non-condensable gases are present in the condenser, the greatest concentration will be at the condenser-subcooler interface. The gas will be carried along to the pump in the form of plugs and can unprime the pump if not removed.

5.0 RECOMMENDATIONS FOR FURTHER TESTING

It is recommended that pressure drop test data be obtained employing more accurate instrumentation such as differential pressure transducers. This should reduce the spread in the data. It would then be practical to pursue further refinements in the two-phase correlation.

The problem of manifolding many condenser tubes together should be investigated. This would also include the stability of parallel tube operation in a gravity-free environment.

Further investigations are required into non-condensable gas removal methods and methods of sealing and degassing a system to prevent the gas problem.

Once a condenser design is conceived based on the results contained in this report and on a system optimization, testing should be initiated with more precision over the desired operation range with apparatus of the same geometry as the actual design.

APPENDIX I

DATA REDUCTION METHODS

1. Correction for momentum change in test condensers.

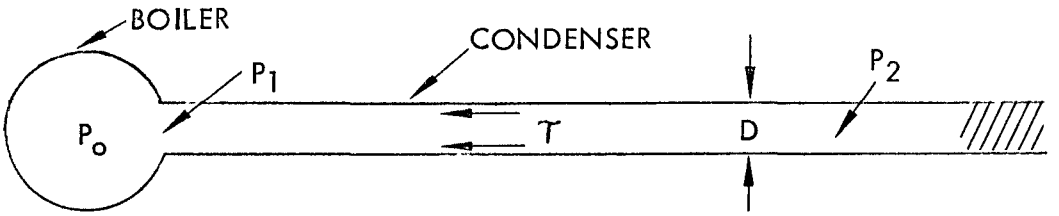

Assume frictionless flow between boiler (Section 0) and condenser inlet (Section 1). Bernoulli equation applies:

$$P_o - P_1 = \frac{\rho_1 U_1^2}{2g} = \tag{1}$$

Steady state momentum equation applies along condenser tube.

$$\Sigma F_x = \int \frac{\rho_2 U_2^2}{g} dA - \int \frac{\rho_1 U_1^2}{g} dA$$

At interface $U_2 \longrightarrow 0$

$$\Sigma F_x = - \frac{\rho_1 U_1^2 A}{g} \tag{2}$$

$$\Sigma F_x = (P_1 - P_2) A - \tau_w \pi DL \tag{3}$$

Equate (2) & (3)

$$- \frac{\rho_1 U_1^2 A}{g} = (P_1 - P_2) A - \tau_w \pi DL$$

$$P_1 - P_2 + \frac{\rho_1 U_1^2}{g} - \tau_w 4 \frac{L}{D} = 0 \tag{4}$$

Substitute P_1 from (1)

$$P_0 - \frac{\rho_1 U_1^2}{2g} - P_2 + \frac{\rho_1 U_1^2}{g} - \tau_w \, 4 \frac{L}{D} = 0$$

$$(P_0 - P_2) + \frac{\rho_1 U_1^2}{2g} = \tau_w \, 4 \frac{L}{D} \qquad (5)$$

Since P_0 and P_2 are measured, add $\frac{\rho_1 U_1^2}{2g}$ to the pressure difference in order to obtain the friction and drag pressure drop.

2. Pressure drop for gas-only

$$dP_g = - \; f \, v \, g \; \frac{G^2}{2g} \; \frac{dL}{D}$$

Assume linear quality change with length

$$x = \left(1 - \frac{L}{L_T} \right)$$

$$dx = - \frac{dL}{L_T}$$

$$dL = - L_T dx$$

$$dP_g = f \, v \, g \; \frac{G^2}{2g} \; \frac{L_T}{D} \; dx$$

$$G = G_o \, x$$

$$v_g = \frac{RT}{P}$$

$$dP_g = \frac{RT}{P}\,\frac{L_T}{D}\,\frac{G_o^2 X^2}{2g}\,dx$$

$$\int_{P_1}^{P_2} PdP = RT\,\frac{LT}{D}\,\frac{G_o^2}{2g}\int_o^1 f\,x^2 dx$$

$$\text{Let}\quad \int_o^1 f\,x^2 dx = f'$$

$$\frac{(P_2^2 - P_1^2)}{2} = RT\,\frac{L_T}{D}\,\frac{G_o^2}{2g}\,f'$$

$$(P_2 - P_1)\frac{(P_2 + P_1)}{2} = RT\,f'\,\frac{G_o^2}{2g}\,\frac{L_T}{D}$$

$$\Delta P_g = P_2 - P_1 = \frac{RT}{\frac{(P_2 + P_1)}{2}}\,f'\,\frac{G_o^2}{2g}\,\frac{L_T}{D}$$

$$\text{Let}\quad \bar{v}_g = \frac{RT}{\frac{(P_1 + P_2)}{2}}$$

Or evaluate $\bar{v}_g$ at average pressure.

$$\Delta P_g = f'\,\bar{v}_g\,\frac{G_o^2}{2g}\,\frac{L_T}{D}$$

$$\text{Now}\quad f' = \int_o^1 f\,x^2 dx$$

Where f is a function of the local Reynolds number.

For $Re < 2000$ $\quad f = \frac{64}{Re}$

$2000 < Re < 4000$ $\quad f = .035$

$Re > 4000$ $\quad f = \frac{.316}{(Re)^{1/4}}$

$$Re = Re_o\, x$$

Therefore if $Re_o > 2000$, f' must be intergrated piecewise

Defining x_1 as the quality where $Re = 2000$ and x_2 where $Re = 4000$ we have

$$f' = \int_o^1 f\, x^2 dx = \int_o^{x_1} \frac{64}{Re_o} \frac{x^2}{x}\, dx + \int_{x_1}^{x_2} .035\, x^2 dx + \int_{x_2}^{1} \frac{.316}{(Re_o)^{1/4}} \frac{x^2}{x^{1/4}}\, dx$$

Performing the integration we have

$$f' = \frac{32}{Re_o} x_1^2 + .011 \left[x_2^3 - x_1^3\right] + \frac{.115}{(Re_o)^{1/4}} \left[1 - x_2^{11/4}\right]$$

This function is plotted in Figure 1-1 where f' is given as a function of inlet Reynolds number.

To compute the pressure drop in a tapered tube, the diameter as a function of length is used in the pressure drop equation and the quality change as a function of length is known from the design. The above procedure can be repeated to find f' and ΔP_g.

The actual condenser pressure drop is: $\Delta P = \Phi\, (\Delta P_g) - \frac{\rho_1 U_1^2}{g}$

GAS-ONLY CONDENSING INTEGRATED FRICTION FACTOR

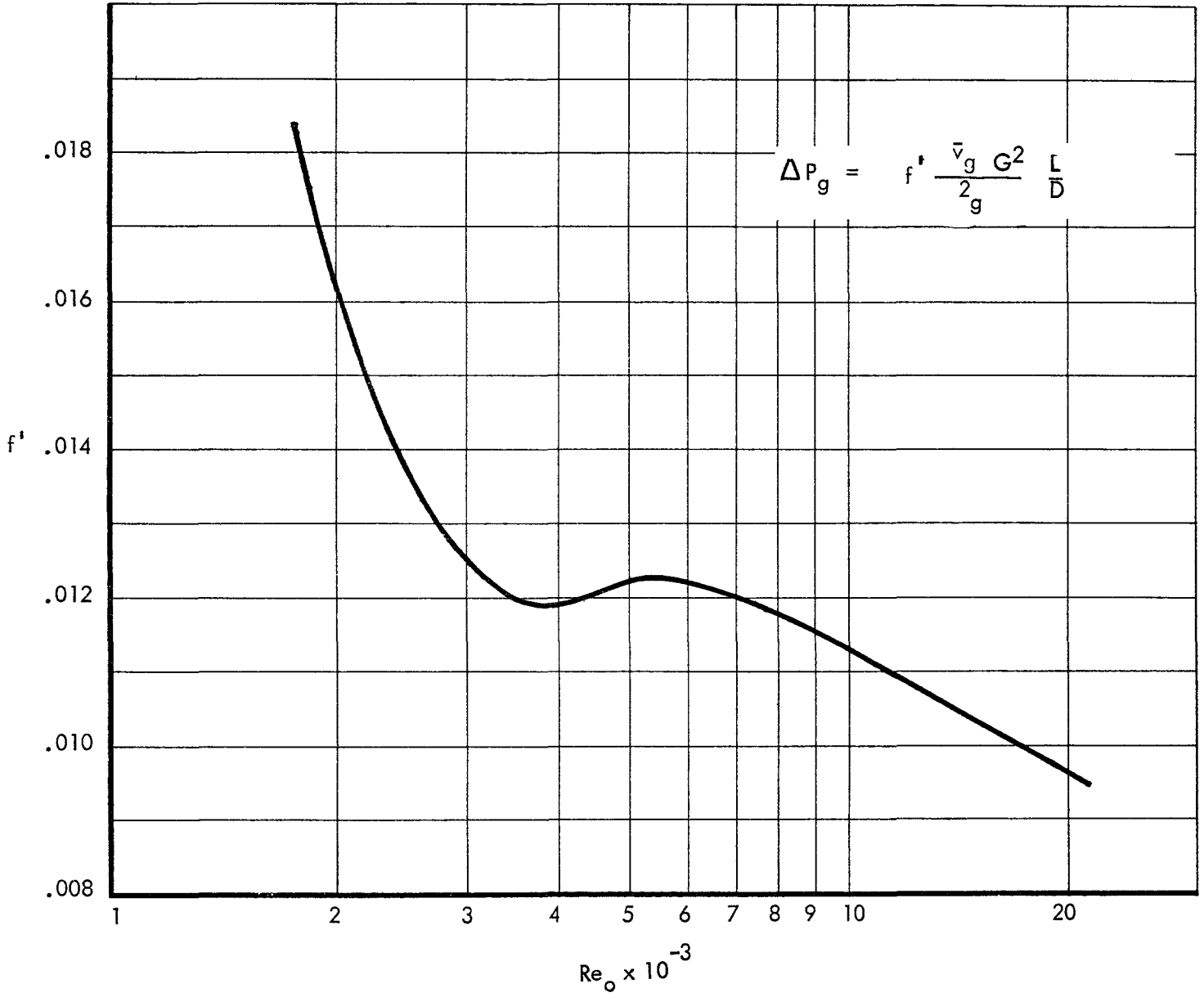

FIGURE I-1

APPENDIX II

CONDENSING TEST DATA

CONSTANT DIAMETER TUBE

0.145 INCH I.D. TUBE HORIZONTAL

P_o PSIA	P_2 PSIA	P_1 PSIA	$\dot{m}$ LB/SEC $\times 10^3$	L_T IN	ΔP_{TP} PSF	$\bar{v}_g$ FT^3/LB	ΔP_g PSF	$Re_o \left(\frac{v_g}{10}\right)^{1.25}$	Φ
5.90	2.73	5.67	1.75	60	491	12.8	232	7,170	2.12
4.96	2.55	4.77	1.55	60	379	14.6	208	7,490	1.82
4.50	2.12	4.13	1.75	60	393	16.9	332	10,200	1.18
4.04	1.90	3.74	1.62	60	352	18.3	285	10,400	1.23
7.46	4.05	7.17	2.22	60	536	9.8	286	6,520	1.87
4.18	1.32	3.91	1.56	60	452	20.0	290	11,200	1.56
4.25	.64	3.90	1.74	60	569	22.5	409	14,400	1.39
3.96	.47	3.57	1.74	60	555	25.0	454	16,400	1.22
3.96	.41	3.74	1.42	60	545	24.6	291	13,200	1.87
3.98	1.29	3.72	1.49	60	424	20.7	271	11,100	1.56

CONSTANT DIAMETER TUBE

0.150 INCH I.D. HORIZONTAL

P_o PSIA	P_2 PSIA	P_1 PSIA	$\dot{m}$ LB/SEC $\times 10^3$	L_T IN	ΔP_{TP} PSF	$\bar{v}_g$ FT^3/LB	ΔP_g PSF	$Re_o \left(\frac{v_g}{10}\right)^{1.25}$	Φ
10.58	8.21	10.37	2.48	65	376	6.18	202	3,950	1.86
11.00	8.75	10.78	2.50	65	359	5.9	197	3,760	1.82
10.67	8.45	10.46	2.50	65	355	6.05	202	3,880	1.76
8.70	4.56	8.21	3.10	65	664	8.7	432	7,580	1.54
7.52	2.90	7.03	2.92	65	735	11.0	487	9,570	1.51
7.52	3.11	7.03	2.90	65	705	10.9	476	9,400	1.48
7.15	2.45	6.62	2.92	65	750	12.0	532	10,700	1.41
7.03	1.02	6.51	2.92	65	940	14.1	622	13,000	1.51
6.91	.46	6.31	3.10	65	1,016	15.5	768	15,600	1.32
8.44	5.50	8.12	2.73	69	474	8.2	340	6,200	1.40
11.48	6.52	11.14	3.03	65	764	6.45	304	5,100	2.51
9.91	2.88	9.09	4.15	65	1,124	9.25	787	10,800	1.43

CONSTANT DIAMETER TUBE

0.150 INCH I.D. HORIZONTAL

P_o PSIA	P_2 PSIA	P_1 PSIA	$\dot{m}$ LB/SEC $\times 10^3$	L_T IN	ΔP_{TP} PSF	$\bar{v}_g$ FT^3/LB	ΔP_g PSF	$Re_o\left(\frac{\bar{v}_g}{10}\right)^{1.25}$	Φ
3.64	0.40	3.34	1.64	65	511	26.9	394	16,500	1.30
3.77	1.63	3.46	1.66	55	351	20.4	260	11,800	1.35
4.06	2.63	3.87	1.45	46.5	236	16.2	132	7,740	1.79
4.36	3.33	4.24	1.40	42	166	14.2	68	6,290	2.44
4.71	4.45	4.62	1.11	33	50	12.1	37	4,110	1.34
5.81	4.98	5.81	.85	22	126	10.1	15.1	2,490	8.34
4.19	1.22	3.77	1.95	65	484	20.6	425	14,000	1.14
4.07	1.92	3.77	1.68	57	351	18.3	246	10,400	1.43
4.48	2.75	4.26	1.62	49	283	15.1	162	7,890	1.75
4.60	3.80	4.42	1.43	42	141	13.0	91	5,770	1.56
5.42	4.92	5.36	1.11	32	85	10.8	35.4	3,570	2.40
2.85	1.69	2.64	1.24	44	198	23.7	131	10,580	1.51
2.79	2.51	2.68	.91	32	56	20.0	47	6,280	1.18
2.35	.69	2.12	1.13	47	271	35.0	174	15,800	1.56
2.76	.64	2.51	1.27	54	340	31.2	223	15,360	1.52
3.48	2.05	3.28	1.35	40	236	19.4	115	9,000	2.05
3.63	.76	3.46	1.54	65	441	24.0	220	13,400	2.00
3.52	1.64	3.20	1.65	55	316	21.1	266	12,200	1.19
3.75	2.46	3.50	1.48	46	220	17.8	149	8,850	1.48
3.92	1.26	3.70	1.48	57	415	20.7	206	10,700	2.02
4.51	.845	4.21	1.79	68	569	22.8	419	14,600	1.38
4.80	.314	4.53	1.83	68	688	21.2	408	13,600	1.68
4.98	.314	4.70	1.83	65	712	20.3	374	12,900	1.90
4.98	.343	4.65	2.02	60	717	20.5	420	14,400	1.71
4.89	.432	4.53	2.08	57	696	20.7	429	15,000	1.62
4.84	.108	4.44	2.10	54	736	22.3	448	16,700	1.64
4.89	.376	4.49	2.15	48	706	21.2	394	16,000	1.79
4.70	.254	4.27	2.09	48	698	22.3	394	16,600	1.77
4.56	.141	4.18	1.47	65	687	23.8	500	16,900	1.37
4.62	.343	4.32	1.78	62	656	22.0	362	13,900	1.81
4.14	.432	3.76	1.87	46	585	24.3	334	16,500	1.75
3.84	.314	3.49	1.79	47	558	26.5	337	17,600	1.65
4.33	1.19	4.01	1.80	65	496	20.0	355	12,400	1.40
4.42	.080	4.05	1.92	60	674	24.8	461	17,400	1.46
4.31	.90	4.04	1.73	65	531	20.8	340	12,600	1.56

HORIZONTAL TAPERED TUBE
(SEE FIGURE 18 FOR GEOMETRY)

P_o PSIA	P_2 PSIA	$\dot{m}$ LB/SEC × 104	L_T IN	ΔP_{TP} PSF	$\bar{v}_g$ FT^3/LB	ΔP_g PSF	$Re_o\left(\frac{\bar{v}_g}{10}\right)^{1.25}$	Φ
4.49	3.72	4.36	16.6	111	13.9	14.2	1,142	7.80
4.64	4.03	4.22	14.5	88.1	12.5	8.95	969	9.15
4.77	4.19	4.86	12.4	83.9	12.1	6.92	1,071	12.2
4.29	3.03	4.18	19.9	182	14.5	21.4	1,156	8.70
4.34	3.56	4.62	18.7	112	13.7	19.3	1,189	5.84
4.44	3.94	4.68	14.7	72.7	12.7	10.4	1,097	7.05
3.66	1.91	4.62	23.5	252	19.0	46.8	1,788	5.84
3.68	2.80	4.30	21.0	126	16.2	27.5	1,367	4.55
3.74	3.50	4.31	14.4	34.9	14.5	10.3	1,192	3.41
2.80	1.94	3.74	20.1	124	21.8	29.5	1,722	4.31
2.98	2.50	3.85	17.7	69.3	19.0	19.6	1,492	3.57
3.12	2.86	3.83	12.3	37.2	17.5	7.57	1,338	4.93
2.88	1.46	4.12	21.4	204	23.5	43.3	2,081	5.30
2.72	1.16	3.93	19.6	224	26.0	39.4	2,257	6.55
2.67	1.56	3.19	18.9	160	24.0	25.2	1,656	6.80
2.64	1.89	2.94	18.9	108	23.0	21.1	1,446	5.14
2.79	1.37	4.10	20.6	205	24.1	41.8	2,136	5.56
3.00	2.20	4.07	18.8	115	20.0	25.4	1,683	4.66
3.41	3.10	4.12	15.5	45.4	16.5	13.4	1,337	3.35
3.68	1.69	4.95	23.3	286	19.5	52.5	1,982	6.20
3.71	2.57	4.73	22.0	164	16.8	34.5	1,571	4.84
4.30	3.35	4.48	19.4	137	14.0	21.0	1,186	6.64
4.49	2.62	5.25	24.3	69.4	15.0	44.0	1,514	6.50
4.63	3.52	5.05	22.8	160	13.1	31.2	1,230	5.24
4.83	4.34	5.00	19.1	70.6	12.0	18.8	1,090	3.68
5.70	1.61	6.62	30.1	589	14.5	78.6	1,830	7.50
5.72	2.28	6.46	29.1	495	13.5	66.0	1,631	7.50
5.75	2.95	6.04	28.0	403	12.5	53.5	1,385	7.55
5.77	3.53	5.88	27.1	322	11.6	44.6	1,228	7.20
6.47	2.60	6.09	31.4	557	12.0	64.5	1,330	8.64
6.63	3.32	6.70	30.4	477	11.0	61.6	1,308	7.75
6.76	4.12	7.23	29.4	380	10.0	56.5	1,255	6.71
7.20	2.96	7.08	32.0	610	10.8	70.7	1,343	8.60
7.39	3.78	7.11	30.9	520	9.9	60.8	1,219	8.55
7.49	4.59	7.20	29.7	418	9.1	52.5	1,111	7.96
7.60	5.40	6.87	28.5	317	8.5	43.0	973	7.38

CONSTANT DIAMETER TUBE 0.157 INCH I.D.

INCLINED UPWARD AT 15° TO HORIZONTAL

P_o PSIA	P_2 PSIA	P_1 PSIA	$\dot{m}$ LB/SEC $\times 10^3$	L_T IN	ΔP_{TP} PSF	$\bar{v}_g$ FT^3/LB	ΔP_g PSF	$Re_o\left(\frac{\bar{v}_g}{10}\right)^{1.25}$	Φ
2.94	2.51	2.94	.508	12	66.2	19.0	7.15	3,242	9.26
3.40	3.23	3.40	.508	13	28.1	16.0	6.52	2,617	4.31
3.88	3.59	3.88	.508	12	44.7	14.2	5.33	2,254	8.39
3.41	3.08	3.41	.684	18	54.2	16.2	12.18	3,561	4.45
3.78	3.45	3.78	.659	16	52.7	14.8	9.54	3,078	5.52
4.12	3.90	4.12	.634	14	35.7	13.1	7.27	2,551	4.91
3.78	3.45	3.78	.731	20	54.2	14.6	13.5	3,417	4.01
4.34	4.10	4.34	.725	14	41.1	12.7	8.09	2,800	5.08
4.73	4.61	4.73	.725	14	22.9	11.8	7.45	2,555	3.07
2.60	1.67	2.60	1.08	34	156.	25.0	68.0	9,790	2.29
3.31	2.88	3.31	.725	26	68.8	17.0	19.9	4,031	3.45
4.02	3.77	4.02	.592	19	39.3	13.8	9.51	2,524	4.13
4.58	4.48	4.58	.408	11	17.0	12.0	3.30	1,467	5.15
2.65	2.56	2.65	.225	10	13.6	20.0	2.83	1,544	4.80
2.84	2.52	2.84	.225	9	47.4	19.5	2.47	1,496	19.2
3.02	2.91	3.02	.225	8	16.9	17.5	1.97	1,304	8.58
3.17	3.05	3.17	.225	7.5	17.4	17.0	1.52	1,260	11.4

TAPERED TUBE INCLINED AT 43° TO HORIZONTAL
(SEE FIGURE 18 FOR GEOMETRY)

P_o PSIA	P_2 PSIA	$\dot{m}$ LB/SEC $\times 10^5$	L_T IN	ΔP_{TP} PSF	$\bar{v}_g$ FT^3/LB	ΔP_g PSF	$Re_o \left(\frac{\bar{v}_g}{10}\right)^{1.25}$	Φ
11.10	10.96	10.0	5.3	19.6	5.1	.044	75	446
9.60	9.35	6.6	6.2	36.4	6.0	.0635	61	574
6.58	6.06	6.8	5.6	75.0	8.4	.0621	95	1207
7.44	7.19	13.3	6.4	35.8	7.5	.177	162	202
6.38	6.25	0.70	5.5	18.1	8.8	.00634	10.2	2860
5.75	5.62	10.8	6.5	18.1	9.8	.204	183	89
5.72	5.43	11.9	6.3	42.1	9.8	.194	202	218
8.28	7.92	22.9	8.0	52.5	6.9	.584	250	90
9.05	8.93	32.5	7.2	17.0	6.4	.550	323	31
8.71	8.37	13.6	6.9	49.0	6.6	.203	140	241
8.85	8.56	12.5	6.2	41.4	6.4	.129	125	320
8.10	8.03	6.6	5.6	10.5	7.0	.050	74	211
6.20	6.05	9.6	5.9	21.7	9.0	.112	146	194

NITROGEN GAS - LIQUID MERCURY

ADIABATIC TWO COMPONENT FLOW TEST RESULTS

$\dot{m}_g$ LB/MIN	X	$\frac{\Delta P_{TP}}{\Delta P_g}$	X_{VT}	$\dot{m}_g$ LB/MIN	X	$\frac{\Delta P_{TP}}{\Delta P_g}$	X_{VT}
.215	.44	1.34	.0425	.150	.20	1.39	.086
	.23	1.54	.068		.06	2.04	.164
	.11	1.93	.108		.03	3.34	.238
	.09	1.97	.117				
	.05	2.45	.159	.50	.63	1.48	.020
	.04	2.50	.181		.33	2.23	.038
	.30	1.50	.058		.10	3.37	.080
	.07	2.35	.138		.06	3.76	.105
	.03	3.05	.202				
	.02	4.11	.241	.75	.74	1.56	.0135
					.46	2.45	.0247
.300	.88	1.14	.021		.30	3.14	.0346
	.48	1.28	.034		.16	3.64	.052
	.17	1.82	.072		.13	3.58	.060
	.14	2.04	.082		.11	3.62	.066
	.19	1.72	.067				
	.15	1.96	.077	1.00	.85	1.36	.0086
	.13	1.99	.083		.61	2.32	.0162
	.12	2.08	.087		.42	3.08	.0238
	.47	1.25	.035		.32	3.49	.0294
	.12	2.11	.088		.27	3.70	.0336
	.05	2.61	.143				
	.03	3.36	.178				
.400	.75	1.10	.0171				
	.41	1.52	.0372				
	.25	1.93	.0504				
	.20	2.20	.0576				
	.17	2.35	.0636				
	.15	2.35	.0685				
	.63	1.36	.0223				
	.16	2.18	.068				
	.06	2.76	.114				
	.04	3.13	.133				

$\dot{m}_g$ = Nitrogen Flow LB/MIN

X = Flowing Quality

X_{VT} = Martinelli Parameter (See Figure 8)

ΔP_{TP} = Two Phase Pressure Drop

ΔP_g = Gas-Only Pressure Drop

Horizontal Tube 0.394 INCH I.D. 4 FT Long

NOMENCLATURE

A	Flow cross sectional area
D	Diameter
F	Force
f	Friction factor
f'	Integrated mean friction factor
g	Gravitational conversion factor
G	Mass flow per unit area
Go	Mass flow per unit area at condenser inlet
L	Length along condenser
L_t	Total condenser length
$\dot{m}$	Mass flow rate
P_o	Total pressure at condenser inlet
P_1	Static pressure at condenser inlet
P_2	Static pressure at condenser outlet
R	Gas constant
Re	Local Reynolds number, vapor
Re_o	Inlet Reynolds number, vapor
T	Absolute temperature
U_1	Condenser inlet vapor velocity
U_2	Condenser outlet vapor velocity
v_g	Vapor specific volume
$\bar{v}_g$	Mean vapor specific volume
X	Flow quality, $\frac{\text{vapor mass flow rate}}{\text{total mass flow rate}}$

ΔP_g, dP_g Vapor only pressure drop

ρ_1 Inlet vapor density

ρ_2 Outlet vapor density

τ_w Shear stress

Φ Ratio of two phase pressure drop to gas only pressure drop

DISTRIBUTION LIST

Advanced Research Projects Agency

Advanced Research Projects Agency
The Pentagon, 3D154
Washington 25, D.C.
Attn: Fred A. Koether

Aerojet General, Azusa

Don Forrest
P.O. Box 573
Azusa, California
Attn: Evelyn Henry/AT(10-1)-880/

Air Technical Intelligence Center

Commander
Air Technical Intelligence Center
Wright-Patterson Air Force Base, Ohio
Attn: H. Holzbauer, AFCIN-4Bla

Air Force Ballistic Missile Division, Inglewood

Air Force Ballistic Missile Division
Hq. Air Research and Development Command
Air Force Unit Post Office
Los Angeles 45, California
Attn: Lt. Col. Melvin M. Burnett, WDAT
(Inside Envelope) For: Major George Austin

Air Force Special Weapons Center

Commander
Air Force Special Weapons Center
Technical Information and Intelligence Office
Kirtland Air Force Base, New Mexico
Attn: Delmer J. Trester

Air University Library

Director
Air University Library
Maxwell Air Force Base, Alabama
Attn: Major Lee C. Free

AiResearch Manufacturing Co. of Arizona

AiResearch Manufacturing Co. of Arizona
P.O. Box 1927
Phoenix, Arizona
Attn: M.H. Currey

Argonne National Laboratory

Argonne National Laboratory
9700 South Cass Avenue
Argonne, Illinois
Attn: Dr. Hoylande D. Young

Army Ballistic Missile Agency

Commanding General
Army Ballistic Missile Agency
Redstone Arsenal, Alabama
Attn: ORDAB-HSI

Atomic Energy Commission, Washington

U.S. Atomic Energy Commission
Technical Library
Washington 25, D.C.
(inside envelope) For: Lt. Col. G.M.Anderson, DRD
Capt. T.L. Jackson, DRD
Lt. Col. C.M. Barnes
R.G. Oehl, DRD
Technical Library

Atomic Energy Commission, California Patent Group

U.S. Atomic Energy Commission
San Francisco Operations Office
2111 Bancroft Way
Berkeley 4, California
Attn: William E. Elliott, Chief
California Patent Group

Bureau of Yards and Docks

Bureau of Yards and Docks (Code 440)
Department of the Navy
Washington 25, D.C.
Attn: Security Officer

Bureau of Naval Weapons

Bureau of Naval Weapons
Department of the Navy
Washington 25, D.C.
Attn: Code RR-12 and RA-8

Bureau of Ships

Bureau of Ships
Code 1500
Navy Department
Washington 25, D.C.
Attn: Melvin L. Ball

Jet Propulsion Laboratory

Jet Propulsion Laboratory
California Insitutute of Technology
Pasadena 3, California
Attn: I.E. Newlan, Supervisor
Technical Reports Dept.

Lawrence Radiation Laboratory

University of California
Lawrence Radiation Laboratory
Technical Information Division
P.O. Box 808
Livermore, California
Attn: Clovis G. Craig
(inside envelope) For: T.C. Merkle

Lockheed MSD, Sunnyvale

Lockheed Missiles and Space Division
3251 Hanover Street
Palo Alto, California
Attn: Miss Kathleen P. Kolan

Chicago Operations Office

Mr. Kenneth A. Dunbar, Manager
Chicago Operations Office
U.S. Atomic Energy Commission
9800 South Case Avenue
Argonne, Illinois
(inside envelope) For: T.A. Nemsek

Chief of Naval Operations

Office of the Chief of Naval Operations (OP-75)
Department of the Navy
Washington 25, D.C.

Continental Army, Command

Office of Special Weapons Developments
U.S. Continental Army Command
Fort Bliss, Texas
Attn: Chester I. Peterson, Capt. AGC

Department of the Army

The Atomic Division
Office of the Chief of Research and Development
Department of the Army
The Pentagon
Washington 25, D.C.

Diamond Ordnance Fuse Laboratories

Commanding Officer
Diamond Ordnance Fuse Laboratories
Washington 25, D.C.
Attn: ORDTL 06.33, Mrs. Elizabeth W. Channel

Institute for Cooperative Research

The Institute for Cooperative Research
University of Pennsylvania
3400 Walnut Street
Philadelphia 4, Pennsylvania
Attn: Dr. Donald S. Murray
Security Officer
TO BE OPENED BY ADDRESSEE ONLY

Los Alamos Scientific Laboratory

Los Alamos Scientif Laboratory
P.O. Box 1663
Los Alamos, New Mexico
Attn: Report Librarian
(Inside envelope) For: Dr. George M. Grover

National Aeronautics and Space Administration, Ames

Ames Research Center
National Aeronautics and Space Administration
Moffett Field, California
Attn: Dr. S.J. Defrance, Director

National Aeronautics and Space Administration, Cleveland

Lewis Research Center
National Aeronautics and Space Administration
21000 Brookpark Road
Cleveland 35, Ohio
Attn: George Mandel

National Aeronautics and Space Administration, Langley

Langley Research Center
National Aeronautics and Space Administration
Langley Field
Hampton, Virginia
Attn: Dr. R.J.E. Reid, Director

National Aeronautics and Space Administration, Washington

National Aeronautics and Space Administration
1512 H Street, N.W.
Washington 25, D.C.
Attn: Dr. Addison M. Rothrock

Naval Ordnance Laboratory

Commander
U.S. Naval Ordnance Laboratory
White Oak
Silver Spring, Maryland
Attn: Eva Liberman

Naval Research Laboratory

Director
Naval Research Laboratory, Code 1572
Washington 25, D.C.
Attn: Mrs. Katherine H. Cass

Oak Ridge National Laboratory

Union Carbide Nuclear Company
X-10 Laboratory Records Department
P.O. Box X
Oak Ridge, Tennessee
(inside envelope) For: Eugene Lamb

Office of Naval Research

Office of Naval Research
Department of the Navy, Code 735
Washington 25, D.C.
Attn: E.E. Sullivan
(inside envelope) For: Code 429

Project RAND

Director, USAF Project RAND
Via: Air Force Liaison Office
The RAND Corporation
1700 Main Street
Santa Monica, California
Attn: F.R. Collbohn
(inside envelope) For: Dr. John Nuth

Rome Air Development Center

Commander, Rome Air Development Center
Griffiss Air Force Base, New York
Attn: RCSG, J.L. Briggs

School of Aviation Medicine

School of Aviation Medicine
Brooks Air Force Base, Texas

Thompson Ramo Wooldridge Inc., Cleveland

Thompson Ramo Wooldridge Inc.
P.O. Box 1616
Cleveland 4, Ohio
Attn: D.L. Southam

Wright Air Development Division

Commander
Wright Air Development Division
Wright-Patterson Air Force Base, Ohio
Attn: WCACT
(inside envelope) For: Capt. Clarence N. Munson WCLEPCNW-1
WCOSI - 2

Technical Information Service Extension, Oak Ridge

U.S. Atomic Energy Commission
Technical Information Extension
P.O. Box 62
Oak Ridge, Tennessee

Chicago Patent Group

U.S. Atomic Energy Commission
Chicago Operations Office
9800 South Cass Avenue
Argonne, Illinois
Attn: George H. Lee

AI Library
Atomics International
P.O. Box 309
Canoga Park, California